PEGylated Polyethyleneimine-Entrapped Gold Nanoparticles for Enhanced and Targeted Gene Delivery Applications

Dissertation submitted to the University of Madeira in order to obtain the degree of Master in Nanochemistry and Nanomaterials

by Yan Zhao

Work developed under the supervision of
Prof. Xiangyang Shi and co-supervised by Prof. Helena Maria Pires Gaspar Tomás

Centro de Competência de Ciências Exatas e de Engenharia,
Centro de Química da Madeira,
Campus Universitário da Penteada, 9000-390 Funchal, Portugal

Julho de 2015

DECLARATION

I hereby declare that this thesis is the result of my own work, is original and was written by me. I also declare that its reproduction and publication by Madeira University will not break any third party rights and that I have not previously (in its entirety or in part) submitted it elsewhere for obtaining any qualification or degree. Furthermore, I certify that all the sources of information used in the thesis were properly cited.

Funchal, July 2015

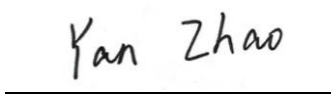

ACKNOWLEDGEMENTS

I am grateful to everyone that directly or indirectly contributed to the execution of this work, especially to my supervisor Prof. Xiangyang Shi and to my co-supervisor Prof. Helena Tomás, for the collaboration and the guidance in my research and for providing the materials and facilities for the development of this project.

I want to thank Rita Castro, Jingyi Zhu and Débora Capelo for all the help and guidance along this one year of the Master project.

I want to thank the NMR technicians, Nilsa Oliveira and Xuedan He, for the help and discussions about 1D- and 2D-NMR.

I want to thank Dr. Carla Alves for all the efforts while I was writing the thesis.

I want to thank Prof. Pedro Pires for the academic discussions about molecular modeling and molecular simulation of polyethylenimine and gold nanoparticles.

I want to thank all other members in CQM, such as Prof. João Rodrigues, Andreia Pimenta, Paula Andrade, Paula Vieira, Catarina Silva, Mara Gonçalves, Dina Maciel, Cláudia Camacho, Manuel Jardim, Carla Miguel and Guoying Wang, for all the help, as well as several visiting students from China, such as Zhe Wang, Benqing Zhou and Zhibo Yu, for academic discussions.

I would like to acknowledge the Portuguese Foundation for Science and Technology (FCT) for funding through the projects PTDC/CTM-NAN/1748/2012, PEst-OE/QUI/UI0674/2014 and the NMR Portuguese Network PTNMR2014/2015. FCT and Santander Bank are also acknowledged for the Invited Chair in Nanotechnology of Prof. X. Shi.

CONFERENCE CONTRIBUTIONS

January/February 2015 – Oral Presentation:

Yan Zhao, Rita Castro, Jingyi Zhu, Helena Tomás, Xiangyang Shi, PEGylated Polyethyleneimine-Entrapped Gold Nanoparticles for Enhanced and Targeted Gene Delivery Applications, presented at the 2nd CQM Annual Meeting/10th Materials Group Meeting – 30th-31st of January 2015 - University of Madeira, Portugal.

ABSTRACT

Gene therapy, which involves the transfer of nucleic acid into target cells in patients, has become one of the most important and widely explored strategies to treat a variety of diseases, such as cancer, infectious diseases and genetic disorders. Relative to viral vectors that have high immunogenicity, toxicity and oncogenicity, non-viral vectors have gained a lot of interest in recent years. This is largely due to their ability to mimic viral vector features including the capacity to overcome extra- and intra-cellular barriers and to enhance transfection efficiency. Polyethyleneimine (PEI) has been extensively investigated as a non-viral vector. This cationic polymer, which is able to compact nucleic acid through electrostatic interactions and to transport it across the negatively charged cell membranes, has been shown to effectively transfect nucleic acid into different cell lines. Moreover, entrapment of gold nanoparticles (Au NPs) into such an amine-terminated polymer template has been shown to significantly enhance gene transfection efficiency.

In this work, a novel non-viral nucleic acid vector system for enhanced and targeted nucleic acid delivery applications was developed. The system was based on the functionalization of PEI with folic acid (FA; for targeted delivery to cancer cells overexpressing FA receptors on their surface) using polyethylene glycol (PEG) as a linker molecule. This was followed by the preparation of PEI-entrapped Au NPs (Au PENPs; for enhancement of transfection efficiency). In the synthesis process, the primary amines of PEI were first partially modified with fluorescein isothiocyanate (FI) using a molar ratio of 1:7. The formed PEI-FI conjugate was then further modified with either PEG or PEGylated FA using a molar ratio of 1:1. This process was finally followed by entrapment of Au NPs into the modified polymers. The resulting conjugates and Au PENPs were characterized by several techniques, namely Nuclear Magnetic Resonance, Dynamic Light Scattering and Ultraviolet-Visible Spectroscopy, to assess their physicochemical properties.

In the cell biology studies, the synthesized conjugates and their respective Au PENPs were shown to be non-toxic towards A2780 human ovarian carcinoma cells. The role of these materials as gene delivery agents was lastly evaluated. In the gene delivery studies, the A2780 cells were successfully transfected with plasmid DNA using the different vector systems. However, FA-modification and Au NPs entrapment were not determinant factors for improved transfection efficiency. In the gene silencing studies, on the other hand, the Au PENPs were shown to effectively deliver small interfering RNA, thereby reducing the expression of the B-cell lymphoma 2 protein. Based on these results, we can say that the systems synthesized in this work show potential for enhanced and targeted gene therapy applications.

Keywords: Polyethyleneimine; Gold Nanoparticles; Gene Delivery; Gene Silencing; Targeting.

RESUMO

A terapia génica consiste na transferência de ácidos nuleicos para células alvo, e é considerada uma das estratégias mais importantes no tratamento de diversas doenças (ex. cancro, doenças infeciosas e distúrbios genéticos). Ao contrário dos vetores virais que têm alta imunogenicidade, toxicidade e atividade oncogénica, os vetores não-virais têm vindo a ganhar notoriedade nos últimos anos. Isto deve-se, em grande parte, à sua capacidade de mimetizar características de vetores virais, como por exemplo a capacidade de superar as barreiras extra e intracelulares e aumentar a eficiência de transfecção. A polietilenimina (PEI) tem sido extensivamente estudado por ser um vetor não-viral. Este polímero catiónico é eficaz na transfeção de diferentes linhas celulares, pois possui a capacidade de condensar os ácidos nucleícos através de interações eletrostáticas e de transportá-los através da membrana celular. Diferentes estratégias têm sido utilizadas para aumentar a eficiência de transfeção deste polímero. A redução de iões de ouro para formação de nanopartículas (Au NPs) no interior deste e outros polímeros semelhantes (com aminas terminais), demonstraram um aumento significativo na eficiência da transfeção de genes por parte destes.

Neste trabalho, foram preparados sistemas de entrega de genes baseados no polímero PEI. Este foi funcionalizado com ácido fólico (FA) (para entrega específica em células cancerígenas alvo, com elevada expressão de recetores FA à superficie) utilizando polietilenoglicol (PEG) como molécula ligante. Em seguida procedeu-se à formação de Au NPs no seu interior (para aumento da eficiência de transfeção). No processo da síntese, isotiocianato de fluoresceína (FI) foi primeiramente ligado às aminas terminais do PEI (razão de 1:7), dando origem a PEI-FI. De seguida, cadeias de polietilenoglicol (PEG) ou polietilenoglicol-ácido fólico (PEG-FA) foram conjugadas ao PEI-FI (razão de 1:1), obtendo-se assim os sistemas finais PEI-FI-*m*PEG e PEI-FI-(PEG-FA). Num passo final, estes sistemas serviram como matriz durante a formação das Au NPs no seu interior. Estes sistemas foram caracterizados por Ressonância Magnética Nuclear, Dispersão Dinâmica de Luz e por espectroscopia de Ultravioleta-Visível para verificar as suas propriedades físico-químicas.

Estudos *in vitro* foram realizados utilizando células de carcinoma do ovário humano (A2780). Estes revelaram que os sistemas PEI-FI-*m*PEG e PEI-FI-(PEG-FA) (com e sem Au NPs) não apresentavam toxicidade. Nos ensaios de entrega de genes, as células A2780 foram transfetadas com sucesso com ADN plásmidico utilizando os diferentes vetores. No entanto, a modificação com FA e a presença de Au NPs não foram factores determinantes para a melhoria da eficiência de transfeção. Por outro lado, os estudos de silenciamento dos genes utilizando pequenos fragmentos de ARN, demonstraram que, os compostos com Au NPs foram capazes de reduzir a expressão da bcl-2, uma proteína presente em células do cancro. Com base nestes resultados, os compostos sintetizados durante este trabalho poderão ser considerados sistemas promissores para aplicações de terapia génica direcionada.

Palavras-chave: Polietilenimina; Nanopartículas de Ouro; Entrega de Genes; Silenciamento Génico; Terapia Direcionada.

CONTENTS

LIST OF ACRONYMS

AbAm	Antibiotic and Antimycotic
Au NPs	Gold Nanoparticles
BCA	Bicinchoninic Acid
bcl-2	B-Cell Lymphoma 2
BSA	Bovine Serum Albumin
DEPC	Diethylpyrocarbonate
DLS	Dynamic Light Scattering
DMSO	Dimethyl Sulfoxide
EDC	1-Ethyl-3-(3-Dimethylaminopropyl)-Carbodiimide
FA	Folic Acid
FBS	Fetal Bovine Serum
FI	Fluorescein Isothiocyanate
$HAuCl_4$	Hydrogen Tetrachloroaurate
*m*PEG-COOH	PEG Monomethyl Ether with a Carboxyl End Group
mRNA	Messenger RNA
MWCO	Molecular Weight Cut-Off
$NaBH_4$	Sodium Borohydride
NH_2-PEG-COOH	Amine-PEG-Carboxylic Acid
NHS	N-Hydroxysuccinimide
NLS	Nuclear Localization Sequence
NMR	Nuclear Magnetic Resonance
N:P	Nitrogen:Phosphate
NPs	Nanoparticles
PAMAM	Poly(amidoamine)
PBS	Phosphate Buffered Saline
pDNA	Plasmid DNA
PEG	Poly(ethylene glycol)
PEI	Polyethylenimine
PVP	Polyvinylpyrrolidone
RES	Reticuloendothelial System
RISC	RNA-Induced Silencing Complex
RLB	Reporter Lysis Buffer
RLU	Relative Light Units
RNAi	RNA Interference
SD	Standard Deviation
siRNA	Small Interfering RNA
TBST	Tris-Buffered Saline/Tween-20
UV-Vis	Ultraviolet–Visible

LIST OF FIGURES

LIST OF TABLES

CHAPTER 1 – INTRODUCTION

CHAPTER 1 – INTRODUCTION

1.1 Nucleic acid delivery

Gene therapy, the transfer of genetic agents into target cells in patients, has become one of the most important and widely explored strategies to treat a variety of diseases, such as cancer, infectious diseases and genetic disorders. Generally, gene therapy is divided into two categories: gene delivery that is the expression of specific proteins through plasmid DNA (pDNA) and gene silencing that is the repression of gene products through small interfering RNA (siRNA). Unlike most peptide and protein delivery systems, nucleic acid delivery systems must deliver nucleic acids to the cytoplasm or to the nucleus of cells. This unique requirement is one of the most significant challenges for applications, since nucleic acid is susceptible to hydrolytic and enzymatic degradation in the body and is not capable of passing through the cell membrane.[1] But it is addressed by using different methods, such as, physical methods, attenuated viral delivery vectors and non-viral delivery vectors. These methods with the respective advantages and disadvantages have great therapeutic potential in a variety of different clinical applications.

1.1.1 Gene delivery

Gene delivery is the process of transferring exogenous DNA into host cells for different applications, such as gene therapy and genetic research. After its transfer, the exogenous DNA is translated intracellularly to specific proteins to perform the corresponding function. Currently, the methods of gene delivery can be divided into three categories: physical methods, non-viral vectors and viral vectors.[2]

Physical methods of gene delivery usually use a physical force to transiently penetrate the membrane barrier of the cells and to promote intracellular gene transfection. These physical forces include electrical, hydrodynamic, mechanical, magnetic and ultrasonic energy.[2] Compared to non-viral and viral vectors, physical methods are very simple, non-immunogenic and display relatively low cytotoxicity,

since the genes are directly delivered into the cytoplasm and nucleus of the cells without any substances that have immunogenic or cytotoxic properties.[3] Physical methods include naked DNA, electroporation, magnetofection, sonoporation and photoporation.

Electroporation is achieved through short electric pulses that temporarily destabilize the cell membrane, generating pores that allow any genes that surround the membrane to penetrate into the cell cytoplasm.[4-5] A limitation to this technique is that the number of transfected cells is few. The parameters of electric pulse, such as, frequency, duration and intensity, can influence gene stability and can induce cell or tissue injury and consequently affect transfection efficiency.[6]

Magnetofection employs a magnetic field and magnetic nanoparticles (NPs) to facilitate gene transfection. These magnetic NPs, which consist of iron oxide coated with cationic materials, can be complexed with nucleic acids through electrostatic interactions. The external magnetic field induces rapid concentrating of the magnetic particles on the target cells.[7-8] After the cellular uptake of nucleic acids by endocytosis and pinocytosis, the magnetic nanoparticles release the nucleic acids into the cytoplasm of the cell through one of several mechanisms which are dictated by the NP composition.[9-10] Important advantages of magnetofection include the localized delivery of nucleic acids to specific areas under the influence of a magnetic field and the improved kinetics of gene transfection even at low dosage.[3]

The sonoporation method utilizes ultrasounds as a physical force to temporarily permeabilize the cell membrane. The resultant formation of pores in the membrane facilitates the cellular uptake of nucleic acids. The parameters of ultrasound, such as, pulse frequency, intensity and duration, as well as the size of the nucleic acid, all play an important role in transfection efficiency.[11-12] Although low transfection efficiency is a disadvantage of this method, the use of ultrasounds is less violent and more comfortable. Thus, it is considered as the preferred physical delivery method for *in vivo* applications.[3]

Photoporation utilizes the femtosecond infrared or near-infrared laser beam to transiently generate some pores in the cell membrane to enhance gene delivery

without any risk of tissue damage.[13-14] Laser density and duration of laser treatment are critical parameters that improve the transfection efficiency of nucleic acids, while a relatively unfocused laser can be used to minimize tissue damage and maximize the transfected area.[13]

Compared to the physical methods and non-viral vectors, viral vectors exhibit relatively high delivery efficiency, especially for gene delivery *in vivo*. This is because viral vectors take advantage of the natural characteristics of viruses to efficiently carry their genome into cells and to navigate into the nucleus. To date, viral vectors include adenovirus, retrovirus, adeno-associated virus, herpes simplex virus, foamy virus, poxvirus and lentivirus. These can be divided into two categories: RNA virus vectors and DNA virus vectors.[15] RNA virus vectors are able to perform permanent transgene expression through gene integration,[16-17] while DNA virus vectors can perform temporary transgene expression in the episomal form without gene integration.[18] Viral vectors, which are different from viruses, are replication deficient viruses that contain the gene sequence of interest but no pathogenic gene sequence from their genome thereby strengthening their safety.[19] But viral vectors still have several problems limiting their applications, for example, immunogenicity, toxicity, side effects in non-targeted cells and costs in production.

1.1.2 Gene silencing

RNA interference (RNAi), an evolutionary conserved gene-silencing mechanism, was discovered in 1998.[20] This procedure employs RNA as the therapeutic agent to carry out RNA silencing that can protect genomes from endogenous and exogenous gene threats and that can control gene expression in cells.[21] Since RNAi possesses ease of manipulation, great specificity and efficiency of gene silencing, it has become a popular and powerful tool for therapeutic applications. Moreover, extensive research in gene delivery has resulted in the development of gene delivery methods and vectors, which offer great potential for the recently emerging gene silencing strategy in which siRNA is delivered intracellularly.[22] Unlike physical methods but similar to DNA

vectors, siRNA vectors can be classified as either viral or non-viral.[23] Compared to non-viral vectors, viral vectors have great silencing efficacy, but their disadvantages, such as immunogenicity, safety and cost limit their development. Non-viral vectors such as cationic polymers and cationic lipids have been designed and synthesized to enhance silencing efficiency. What is more, relative to DNA vectors, siRNA vectors are not required to deliver siRNA into the nucleus but only into the cytoplasm. After delivery into the cytoplasm, siRNA can be used to perform gene silencing.

In the general process of gene silencing (Figure 1), long double-stranded RNA molecules are cleaved into 21-23 siRNA nucleotide fragments by the endogenous RNaseIII-like enzyme, Dicer.[24] The resulting siRNA molecules are incorporated into the RNA-induced silencing complex (RISC), which includes proteins necessary for unwinding the siRNA as well as binding and cleaving the target messenger RNA (mRNA).[25] After activation of the formed RISC-siRNA complex, the siRNA is unwrapped and one of the two strands is released, consequently leading to the formation of the RISC complex with a single RNA strand. The activated RISC-RNA complex binds to the homologous target mRNA by specific base-pair recognition, resulting in the sequence-specific degradation of mRNA and finally the knock-down of the expression of the corresponding protein.

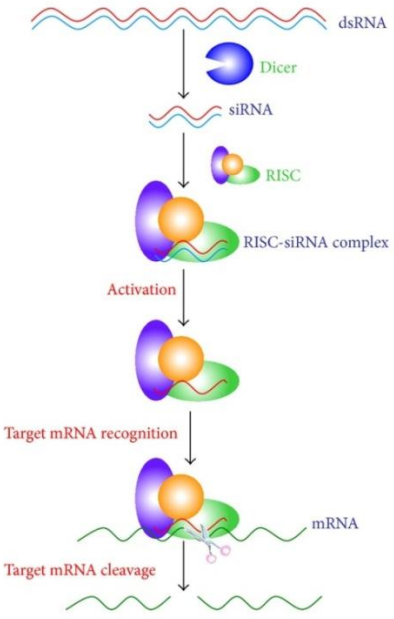

Figure 1 The mechanism of RNAi. (Figure adapted from Ref. 26)

1.1.3 Delivery mechanism of non-viral vectors

In nucleic acid delivery systems, there are a variety of both extracellular and intracellular barriers, which decrease the probability of nucleic acid entry into the cytoplasm or the nucleus. The extracellular barriers include degradation by nucleases, non-specific interaction with biomacromolecules, uptake by the reticuloendothelial system (RES), renal excretion and diffusion from the extracellular matrix to the cell surface. Several hurdles must be overcome in the intracellular aspect including cellular binding, uptake and internalization, lysosomal degradation, as well as nuclear localization.[1, 22]

As efficient vectors, viruses can overcome the above barriers, through different functions, for example, protection of nucleic acid, intracellular and extracellular transport, endolysosomal escape, internalization and targetability. By imitating virus features, non-viral vectors have been rationally designed to overcome these barriers and to achieve the goal of effective nucleic acid delivery for enhanced efficiency.[1] The delivery mechanism of non-viral vectors for gene delivery and gene silencing are simply described and compared below.

Due to the anionic property of nucleic acids (DNA and RNA), non-viral vectors should be cationic in nature in order to bind and condense the nucleic acid by electrostatic interaction to form compact complexes.[27] An excessively cationic vector is required to neutralize the negative charge of the nucleic acid and to form the positive complexes. The resultant complexes with net positive charge can interact with the negatively charged cellular membrane and can be internalized into the cells through different pathways (e.g., receptor mediated endocytosis or adsorptive endocytosis) as shown in Figure 2. After cellular uptake, the siRNA can directly escape from the endosomal compartment and then perform gene silencing. In the case of DNA, during maturation of the endosome to a lysosome, the nucleic acid is easily degraded by enzymes in the acidic environment. Here, not only can the cationic vector protect the DNA from degradation but it can also facilitate the escape of the polyplexes from the endosomal or lysosomal compartments through a mechanism,

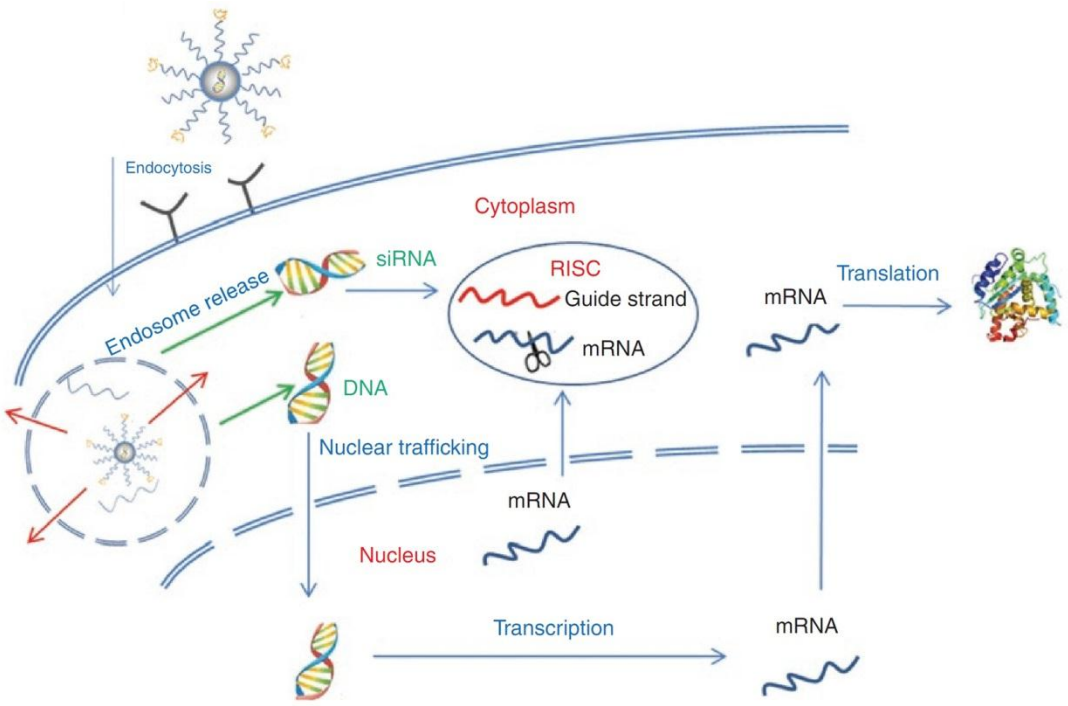

Figure 2 Representative scheme of nucleic acid delivery. RISC: RNA-induced silencing complex; siRNA: small interfering RNA; mRNA: messenger RNA. (Figure adapted from Ref. 28)

such as the proton sponge effect.[29] After arriving at the cytoplasm, the polyplexes start to move towards the nucleus through passive diffusion or a nuclear translocation process.[30-32] Finally, after the DNA is released from the polyplexes into the nucleus, transcription and translation are carried out to express the targeted proteins.

1.1.4 Targeted nucleic acid delivery

In order to enhance the concentration of nucleic acid at the site of action and to spare widespread toxicity at non-target sites, active and passive targeting strategies have become more essential in clinical applications.

Due to the specific physiology of organs or tissues, as well as the properties of the vectors, the tendency of complexes to accumulate in a specific organ has been used as a passive targeting strategy. This process is commonly influenced by the size and surface features of the complexes.[33] It has been shown that complexes larger than 100 nm are easily taken up by the RES and then accumulated in the spleen, while

complexes less than 10 nm in size are easily eliminated by the kidneys. Complexes of 10-100 nm, particularly those smaller than 70 nm, tend to accumulate in the liver through fenestrated capillaries. Complexes smaller than 200 nm in size effectively accumulate in solid tumors through prolonged circulation time and the enhanced permeability and retention effect, which depends on the leaky nature of the tumor vasculature.[1, 34]

Compared to viral vectors, non-viral vectors lack cellular binding and internalization selectivity. To overcome this limitation, a variety of moieties that target specific tissues or cells can be conjugated onto the non-viral vectors. Moieties such as folic acid (FA),[35] mannose,[36] galactose,[37] integrin-binding peptide,[38] transferrin,[39] antibodies,[40] vitamins[41] and aptamers[42] have been shown to enhance cellular uptake efficacy in certain cells or tissues, including dendritic cells,[36] cardiovascular tissue,[43] skeletal muscle[44] and airway epithelium[45]. Moreover, these moieties have been shown to decrease the potential side effects associated with the vectors in other tissues or cells.[46] Compared with other targeting moieties, antibodies possess distinct advantages, such as, high affinity, high specificity and flexibility in selectivity. However, as these moieties are biological macromolecules, they may produce an immunogenic response. Thus, if receptors are overexpressed on the target cells, the use of small molecules as targeting moieties is a judicious choice.[47]

In gene delivery, the nuclear envelope is one of the intracellular barriers that must be overcome by non-viral vectors. As pDNA is unable to passively diffuse through the nuclear pore complex, nuclear entry can occur via two major routes. The first is through passive nuclear importation during mitosis, where the nuclear membrane temporarily breaks down; while the second route of nuclear entry can occur via active transport through the nuclear pore complex.[48] Whether nuclear entry of polyplexes with polyethylenimine (PEI) relies on cell division is under debate.[49-55] For gene delivery of PEI-based polyplexes in nondividing cells, the transport of pDNA from the cytoplasm into the nucleus can be improved by electrostatically complexing or covalently conjugating the nuclear targeting function of synthetic

nuclear localization sequence (NLS) peptides,[56] ketalization[57] and oligosaccharides[58] onto the polymer. In the case of nuclear targeting using gold nanoparticles (Au NPs), conjugation with NLS peptides has also proved to be a successful strategy.[59] Au NP constructs made up of nucleolin-specific aptamers and gold nanostars have also been shown to be actively transported to the nucleus via nuclear envelope invaginations, resulting in major changes in nuclear phenotype and increasing therapeutic efficacy.[60] More recently, the size-dependent intranucleus delivery of ultrasmall Au NPs (smaller than 10 nm) was reported as a novel strategy for nucleic acid delivery.[61] Moreover, studies have indicated that PEI-capped Au NPs may be used as nuclear-targeting vectors for gene delivery.[62]

1.2 Non-viral vector systems

In gene therapy applications, the simplest approach is to use the "naked" gene without any carriers. However some problems, such as little uptake by the cells, speedy degradation by the nucleases and rapid clearance from the plasma, have limited the development of this approach. In order to overcome these problems, as well as those associated with the physical methods and viral vectors discussed in Section 1.1, non-viral vectors provide an attractive alternative approach. For a desirable non-viral vector, several requirements should be met. The vector should be able to (1) prevent degradation of the nucleic acid during systemic circulation, (2) efficiently deliver the nucleic acid to the target site, (3) facilitate the cellular uptake and endosomal escape of the nucleic acid, and (4) either release siRNA to the cellular RNAi machinery or release pDNA to the nucleus.[63] Moreover, the non-viral vector should be non-immunogenic, non-pathogenic, non-toxic, inexpensive, easily administrable and stable.[27]

The majority of non-viral vectors can be divided into cationic lipids and cationic polymers, whose complexes with pDNA are known as lipoplexes and polyplexes, respectively. Cationic lipids used as gene delivery vectors were first reported in 1987 by Felgner.[64] Cationic lipids have relatively high efficiency and a wide range of

applications. However, disadvantages, such as low reproducibility, instability and toxicity, are particularly outstanding and limit their applications. Cationic polymers, such as PEI, chitosan, dendrimer and poly(L-lysine), have been widely studied, but high cytotoxicity and low transfection efficiency are properties that have lowered their potential use in clinical applications.[65] On this basis, smart cationic polymers with desirable properties have been designed and synthesized as non-viral gene delivery vectors, which are chemically stable in the extracellular environment and are rapidly degradable in the intracellular environment.[1, 66] Additionally, inorganic materials with multifunctional properties have also been exploited as novel non-viral vectors for gene therapy (e.g. Au NPs, carbon nanotubes, quantum dots, superparamagnetic iron oxide NPs and silica).[67]

1.2.1 PEI

PEI was investigated as a versatile synthetic vector for gene and oligonucleotide transfection in 1995,[29] and has since been one of the most commonly and popularly employed non-viral cationic nucleic acid vectors with superior transfection consistency and efficiency both *in vitro* and *in vivo*.[28, 68] As a high charge density polycation, PEI has repeating units in which there is a protonable amino-nitrogen in every three atoms. Typically, PEI can be divided into three types: linear PEI, branched PEI and PEI dendrimer, as shown in Figure 3. Linear PEI contains all secondary amines only. In contrast, branched PEI contains not only primary and secondary amines, but also tertiary amines, two-thirds of which are protonated under physiological conditions. The remaining unprotonated tertiary amines of branched PEI have different pKa values that confer a large buffering capacity (representing the percentage of amino groups that become protonated from pH 7.4 to 5.1).[29, 69] This property of high buffering capacity at low pH led to the proton sponge hypothesis proposed by Behr in 1997,[70] in which as PEI molecules are pumped into the endosomes, more protons than unprotonated amines of the polymer absorbed are also pumped into and increase the massive influx of chloride ions and water into the

endosomes. The cooperative effect of osmotic swelling and the swelling of PEI induced by the steric repulsion between protonated amines induces endosomal membrane rupture, facilitating the escape of the polyplexes from the endosomal compartment to the cytoplasm during the maturation of the endosome into a lysosome.[70-71] Thus, buffering capacity is one of the most important parameters that can be used to evaluate the ability to mediate endosomal escape. More recently however Benjaminsen et al. pointed out that PEI does not induce the change in lysosomal pH value and it is unlikely that the proton sponge effect is the principal mechanism of polyplex release.[72]

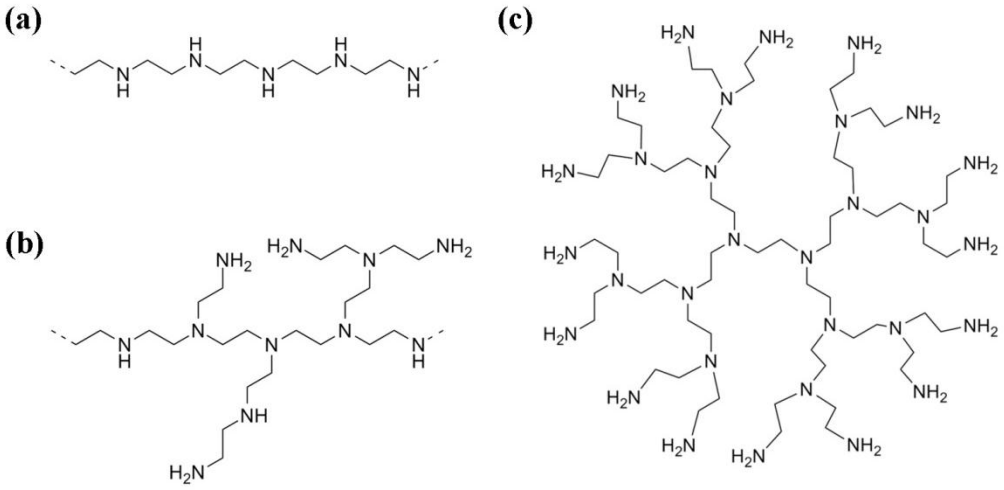

Figure 3 Schematic illustration of the structure of (a) linear PEI fragment, (b) typical branched PEI fragment and (c) PEI dendrimer generation 4. (Figure adapted from Ref. 73)

As a nucleic acid non-viral vector, PEI has an inherent disadvantage in that it is highly cytotoxic *in vitro*. There are two kinds of cytotoxicity mechanisms during the PEI mediated transfection procedure.[74-75] In the first mechanism, the cellular membrane may be destabilized by free PEI, which results in necrosis-related cytotoxicity. The removing of free PEI from the polyplexes may lead to a decrease in their cytotoxicity.[76] In the second mechanism, free intracellular PEI that is dissociating from the polyplexes can bind to the negatively charged mitochondrial membrane, which leads to harmful cellular apoptosis. If PEI can be degraded into small pieces in the cell, the cytotoxicity induced by PEI could be decreased. Moreover, the molecular weight of PEI has an influence on cytotoxicity and transfection

efficiency. Compared to high molecular weight PEI, low molecular weight PEI possesses inferior cytotoxicity and lower transfection efficiency.[77]

A compromise between cytotoxicity and transfection efficiency is one of the primary parameters that should be taken into account. Generally, the conjugation of poly(ethylene glycol) (PEG) onto PEI is a useful method to produce PEGylated PEI with lower cytotoxicity, lower aggregation and higher stability.[78] Although PEGylated PEI shows lower cytotoxicity and has a positive surface charge to compact pDNA to form polyplexes, PEGylation usually decreases transfection efficiency. This is because PEGylation not only decreases the surface charge of the polyplexes thereby attenuating cellular internalization and endosomal escape of polyplexes,[79] but it also forms a distinct hydrated layer which is a result of the steric shielding effect of PEG.[80] In order to attain the best compromise, the molecular weight of PEI and PEG and the ratio between them should be optimized. Besides PEGylation, attempts have been made to reduce the cytotoxicity of PEI through other modifications of its primary amines, for example, N, N-dimethylaminoethl methacrylate,[81] dextran,[82] cationic lipid,[83] cystamine derivatives[84] and N-isopropylacrylamide.[85]

1.2.2 Au NPs

Currently, nanotechnology is considered to hold great promise in the development of novel agents for various biomedical applications. In fact, it is an active field in which numerous nanomaterials including nanoparticles, nanotubes, nanorods and nanowires can be obtained by “top-down” or “bottom-up” approaches. Nanoparticles, particles with a diameter of 1 to 100 nm in two or three dimensions, have attracted a lot of attention. Au NPs in particular possess significantly useful characteristics, such as a high surface-to-volume ratio, size- and shape-dependent properties, ease of surface functionalization, low cytotoxicity and remarkable biocompatibility. These NPs exhibit a wide range of excellent physical and chemical properties, for example, surface-enhanced raman scattering, surface plasmon resonance, fluorescence quenching, magnetic resonance, redox activity and catalytic activity, all of which are different from those of the same bulk material or atom.[86-88]

Surface plasmon resonance in particular results in the unique optical properties of Au NPs, a feature that forms the basis of several biomedical applications and that can be tailored by varying the shape or size of Au NPs.[89] The size distribution and morphology of Au NPs can be analyzed and characterized by using different analytical techniques, for example, ultraviolet–visible (UV-Vis) spectroscopy, dynamic light scattering (DLS), X-ray diffraction, small-angle X-ray scattering, electron microscopy, scanning probe microscopy and mass spectroscopy.[90]

Based on distinct properties discussed above, Au NPs have been applied in several medical and biological fields including targeted delivery of small- and macro-molecular drugs, biosensors, immunoassays, bioimaging of cells and tissues, detection and photothermal therapy of cancer cells and microorganisms (Figure 4). In order to achieve the synergistic effects of the properties of Au NPs and the function of capping ligands, multi-functional capping ligands have been loaded onto Au NP surfaces through non-covalent conjugation (i.e., hydrophobic interactions, electrostatic interactions and specific binding affinity) and covalent conjugation (i.e., thiolation, click chemistry reaction and amine-carboxylate binding).[91-96] This synergistic effect makes Au NPs significantly versatile for biomedical applications. As a non-viral vector, Au NPs have attracted much attention because of their low toxicity, bio-inertness, ease of synthesis and ease of surface modification.

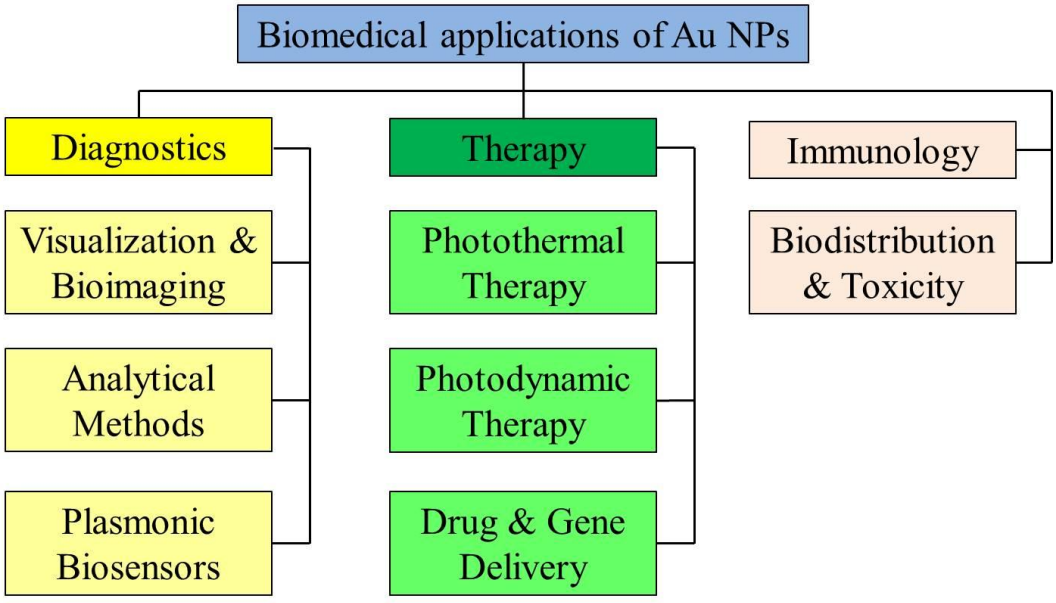

Figure 4 Scheme for the biomedical applications of Au NPs. (Figure adapted from Ref. 97)

1.2.2.1 Classical synthesis of Au NPs

Au NPs have been successfully synthesized for different applications using applied methods, such as sonolysis, laser radiation, chemical reduction and gas condensation. But in medical and biochemical applications, Au NPs are supposed to be soluble in aqueous solution. Thus, chemical reduction is considered to be the most important and appropriate synthesis method.

One of the most popular synthesis methods for preparing Au NPs is called the Turkevich method that was developed by Turkevich et al. in 1951.[98] In this method, hydrogen tetrachloroaurate ($HAuCl_4$) in boiling water is treated with citric acid, which not only reduces the gold ions to atoms but also stabilizes the colloidal Au NPs. Frens further improved this method by changing the relative amounts of the gold/citrate reactants, in order to control the size distribution of the Au NPs through adjusting the relative rates of the two independent processes of nucleation and growth of the Au NPs.[99] These citrate-stabilized Au NPs have been used as tunable foundational materials for a variety of applications, since the ligand exchange of functionalized thiols for them was carried out.[100] In the process of the exchange of the thiolate ligand, several agents, including Tween 20[101] and thioctic acid,[102] have been successfully used to overcome the irreversible aggregation of electrostatically stabilized NPs in water.

In 1994, Brust et al.[103] created a novel one-step method for the preparation of unusual Au NPs by combining a two-phase approach[104] and monolayer self-assembly with alkane thiols.[105-106] Here, $AuCl_4^-$ was transferred from water to toluene by using the phase-transfer reagent tetraoctylammonium bromide and was then reduced with sodium borohydride ($NaBH_4$) in the presence of the thiol capping ligand dodecanethiol, resulting in surface reaction in both nucleation and growth of Au NPs. In this simple method for the direct synthesis of surface-functionalized Au NPs, the reaction conditions can be changed to fabricate low dispersity Au NPs with core diameters of 1.5 to 5.2 nm. Also, owing to both the strong gold-thiol interactions and

the van der Waals attractions between the neighboring ligands, these Au NPs possess higher stability relative to others.[107-108]

1.2.2.2 Templated synthesis of Au NPs

Unlike the irreversible aggregation of electrostatically stabilized Au NPs in water, alkanethiolate-stabilized Au NPs are so stable and dispersible both in organic and aqueous media as a result of steric repulsion. In the spontaneous modification of capping ligands onto the surface of the gold core, efficient bonding interactions are needed. In fact, bonding between the Au atoms and organic molecules that contain either sulfhydryl, amine or carboxyl groups can form S-Au, N-Au or O-Au bonds, respectively, which play a role in stabilizing the Au NPs.[109-111] Generally, Au NPs can be generated by using reducing agents. Not only may these two kinds of agents need different reaction conditions, but also excessive reducing ions added during the reducing process may not be fully removed. Based on this, templated synthesis methods have attracted tremendous attention to enhance the homogeneity and purity of the Au NPs.

As a template, a polymer with reducing ability can be used to reduce and stabilize Au NPs, and even control their size and shape. This can be achieved by regulating the polymer structure and reaction conditions using any one of the four categories: nonelectrolyte homo-polymers, dendrimers, polyelectrolytes, and block copolymers.[112]

As a water-soluble nonelectrolyte homo-polymer, polyvinylpyrrolidone (PVP) was used by Zhou et al. to synthesize extremely stable non-toxic size-controlled water-soluble monodispersed Au NPs.[113] Here, sodium hydroxide was used as the initiator in a one-step reaction method at room temperature and the reaction reached completeness in several minutes.[113] Overall, the possible reducing mechanisms of PVP can be divided into three categories: C=O double bond, free radical mechanism and the oxidation mechanism of the hydroxyl end groups.[114-117] As shown in Figure 5,

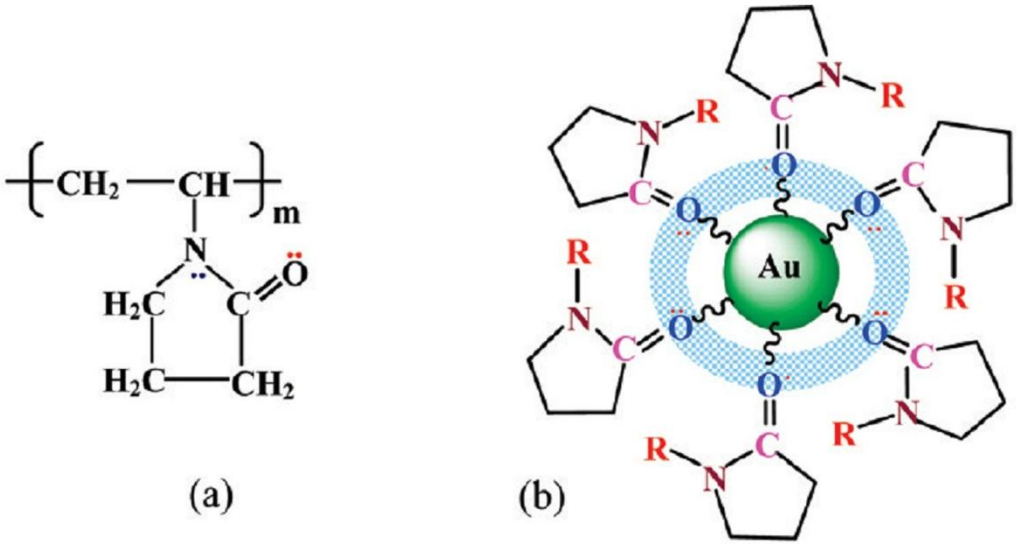

Figure 5 Adsorption and cobridging of (a) PVP molecules in (b) a surface layer via Au atoms on a gold particle. (Figure adapted from Ref. 118)

the C=O oxygen atoms of PVP can be easily attached to the surface of Au NPs through a strong adhesive force.[118] Thus, PVP can be considered as an ideal stabilizer that protects Au NPs from agglomeration and that directs Au NPs growth.

Dendrimers have well-defined three-dimensional molecular architectures with multiple surface functional groups and a low polydispersity index.[119] As a template, amine-terminated poly(amidoamine) (PAMAM) dendrimers have been used to entrap or stabilize Au NPs,[120] the size of which can be controlled by the gold atom/dendrimer ratio[121] or the dendrimer generation.[122] In the reaction, a slow reduction rate can be used to form a hybrid dendrimer-metal composite material.[123]

Electrolyte polymers such as PEI, which have good water-solubility and reducing capacity, can be used to synthesize Au NPs in aqueous solution. In the synthesis process, the cationic polyelectrolyte PEI can be used as a stabilizer and a reducing agent, due to the reducing effect of its amino end groups. The molar ratio of PEI to Au precursors has influence on the growth of the Au NPs, resulting in the different sizes of the formed nanoparticles.[124-126] The PEI-stabilized Au NPs have less cellular toxicity and were shown to be suitable for carrying siRNA.[127] Compared to the irregular structure of PEI, the design of block copolymer structures can meet the

requirements necessary to improve the surface chemistry characteristics and to control the size and the solubility of the formed Au NPs. Moreover, by using a bottom-up "cage-to-framework" method, a well-defined, discrete organic molecular cage with pendant interior thioether groups was recently used in the controlled synthesis of Au NPs inside a cage cavity exhibiting a narrow size distribution (1.9 ± 0.4 nm).[128]

1.2.3 Gold/PEI non-viral vector

Since the limited characteristics of inorganic or polymeric materials may not satisfy the needs of more diverse applications, such as theranostic agents,[129] more and more attention has been paid to inorganic/polymeric hybrid system in order to achieve the synergistic effects of the properties of inorganic materials and the functions of polymeric materials. For non-viral vectors, the synergistic effects may lead to a reduction in cytotoxicity, an increase in transfection efficiency, a targeting ability and the use of a low-dose.[67, 130] For instance, Shan et al. reported[119] that amine-terminated generation 5 PAMAM dendrimers were utilized as templates to synthesize Au NPs with different gold atom/dendrimer molar ratios (Figure 6). The formed dendrimer-entrapped Au NPs were demonstrated to be effective non-viral gene delivery vectors that possessed significantly higher gene transfection efficiency relative to the dendrimers without entrapped Au NPs. Entrapment of the Au NPs within the dendrimers helped preserve their 3-D spherical morphology resulting in a more efficient interaction between the dendrimers and pDNA. Moreover, these non-viral vectors were shown to possess the low cytotoxicity when compared with the native generation 5 PAMAM dendrimer.[35, 119]

In the case of gold/PEI hybrid systems that are used as non-viral vectors, PEI has generally been constructed onto Au NP cores, which are known to provide an applicable and attractive scaffold for nucleic acid delivery.[131-132] Au NPs can be synthesized with a diameter of about 5 to 150 nm and can then be modified with surface ligands that endow the Au NPs with specific properties.[131, 133] In several defferent studies, branched PEI polymers having different molecular weights (2 kDa and 0.8 kDa) were conjugated onto Au NPs to form PEI-capped Au NPs.[131, 134-135]

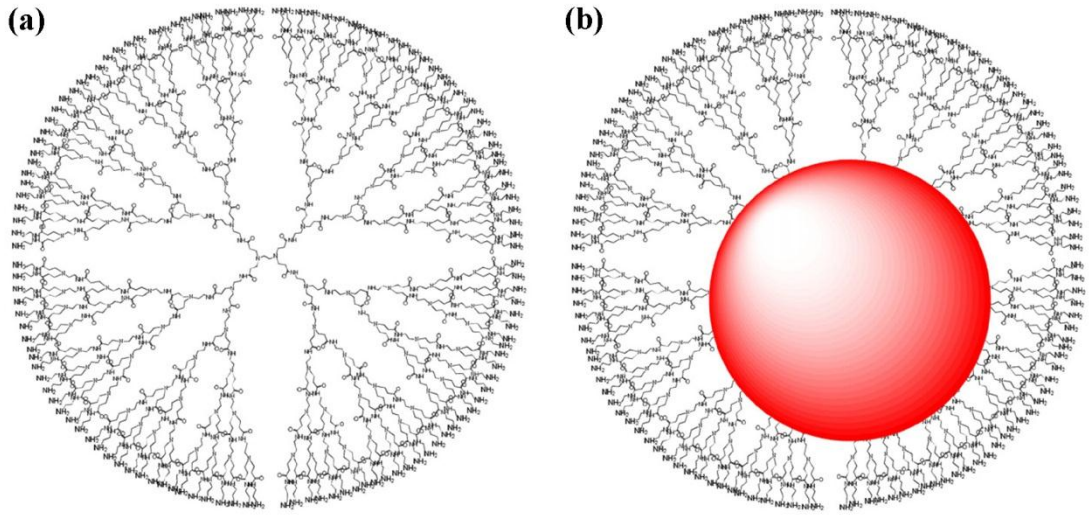

Figure 6 Schematic illustration of the structure of (a) amine-terminated generation 5 PAMAM dendrimers and (b) dendrimer-entrapped Au NPs. (Figure adapted from Ref. 119)

The prepared materials were all shown to exhibit high transfection efficiency, mild cytotoxicity and potential clinical applications as gene delivery vectors.[131, 134-135] In another study it was found that by conjugating pDNA expressing short hairpin RNA onto similar PEI-capped Au NPs, the nuclear-targeting vector was able to downregulate target genes expressed in the nucleus.[62] PEI-capped Au NPs synthesized using high molecular weight PEI (25 kDa) by reductive catechol chemistry or by a one-pot synthesis method have also been prepared and subsequently evaluated as gene silencing vectors.[127, 136] These vectors, which were conjugated with monoclonal antibodies to endow them with targeting capabilities, displayed extremely low cytotoxicity and high gene silencing efficiency.[137] PEI-capped Au NPs used as a core and then coated with multiple alternating layers of positively charged polyelectrolytes and negatively charged genes using a layer-by-layer approach, led to the development of vectors capable of simultaneous co-delivery of pDNA and siRNA.[130, 138]

1.3 Objectives of the thesis

The main objective of the present project was to develop a novel non-viral nucleic acid vector for enhanced and targeted nucleic acid delivery applications. The

system to be developed was based on the entrapment of Au NPs in PEGylated PEI, thereby forming Au PENPs. In the synthesis process (Figure 7), the primary amines of PEI were first partially modified with FI. The resulting conjugates were then either partially PEGylated or modified with PEGylated FA to get the PEI-FI-*m*PEG and PEI-FI-(PEG-FA) conjugates. Lastly, these conjugate systems were used as templates to entrap Au NPs to produce the corresponding Au PENPs. The synthesized conjugates, as well as their respective Au PENPs, were analyzed and characterized using different techniques including UV-Vis spectroscopy, DLS and nuclear magnetic resonance (NMR). They were then finally evaluated *in vitro* as non-viral vectors for the enhanced delivery of either pDNA or siRNA using A2780 human ovarian carcinoma cells that overexpress FA receptors.

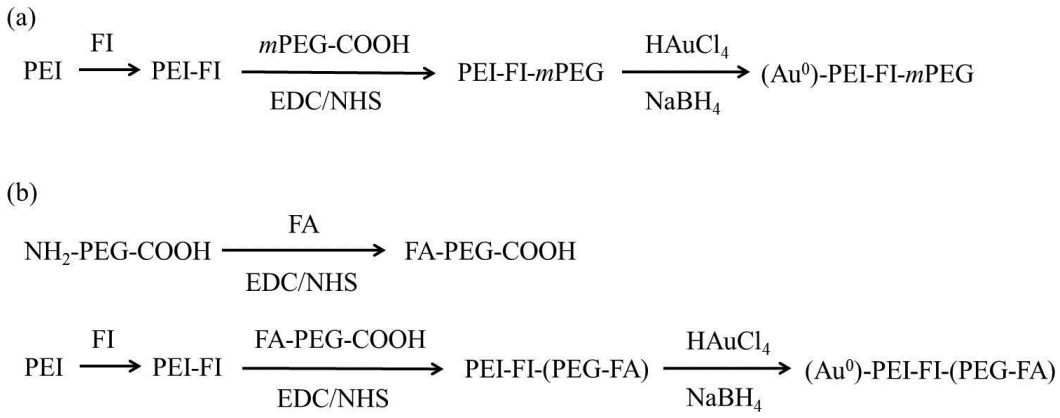

Figure 7 Synthesis procedures of (Au^0)-PEI-FI-*m*PEG (a) and (Au^0)-PEI-FI-(PEG-FA) (b).

CHAPTER 2 – MATERIALS AND METHODS

CHAPTER 2 – MATERIALS AND METHODS

2.1 Materials and reagents

Branched PEI (Mw = 25 kDa), fluorescein isothiocyanate (FI), FA, $NaBH_4$, 1-ethyl-3-(3-dimethylaminopropyl)-carbodiimide (EDC), *N*-hydroxysuccinimide (NHS) and $HAuCl_4$ were purchased from Sigma-Aldrich (MO, USA). PEG monomethyl ether with a carboxyl end group (*m*PEG-COOH, Mw = 2 kDa) and amine-PEG-carboxylic acid (NH_2-PEG-COOH, Mw = 2 kDa) were from Shanghai Yanyi Biotechnology Corporation (China). Spectra/Por® regenerated cellulose dialysis membranes (molecular weight cut-off, MWCO = 1 kDa and 10 kDa) were acquired from Spectrum Laboratories, Inc (CA, USA). Reporter lysis buffer (RLB) and the luciferase assay system were from Promega (WI, USA). The PicoGreen assay kit, fetal bovine serum (FBS) and RPMI-1640 medium were purchased from Invitrogen. siRNA for b-cell lymphoma 2 (bcl-2) was acquired from Ambion® (TX, USA). The GenElute™ Endotoxin-Free plasmid maxiprep kit was acquired from Sigma-Aldrich (MO, USA). The enhanced chemiluminescence western blotting detection kit was acquired from Amersham (Amersham, UK). All other reagents used in this work were obtained from Sigma-Aldrich (MO, USA).

2.2 Synthesis and characterization of Au PENPs

2.2.1 Synthesis of PEI-FI-*m*PEG conjugate

According to a previous report,[139] the PEI-FI conjugate was synthesized with a FI:PEI molar ratio of 7:1. FI in 5 mL dimethyl sulfoxide (DMSO) solution (3.27 mg, 8.40 mmol) was added dropwise into a solution of PEI dissolved in 5 mL DMSO (30.00 mg, 1.20 mmol) under vigorous magnetic stirring at room temperature overnight. The reaction mixture was dialyzed against phosphate buffered saline (PBS) (3 times, 2L) for 1.5 days and distilled water (3 times, 2L) for 1.5 days through a 1000

MWCO membrane to remove the excess of reactants. This was followed by lyophilization.

Using the prepared PEI-FI conjugate, PEI-FI-*m*PEG conjugates were synthesized with *m*PEG:PEI molar ratios of 1:1. The COOH group of *m*PEG-COOH (2.40 mg, 1.20 mmol) was first activated with EDC (2.30 mg, 12.00 mmol) and NHS (1.38 mg, 12.00 mmol) in 3 mL DMSO at room temperature for 3h. The resulting solution of activated *m*PEG-COOH was added dropwise into a solution of PEI-FI dissolved in 5 mL DMSO under vigorous magnetic stirring at room temperature for 3 days. The reaction mixture was dialyzed against PBS (3 times, 2L) for 1.5 days and distilled water (3 times, 2L) for 1.5 days through a 10000 MWCO membrane to remove the excess of reactants. This was followed by lyophilization.

2.2.2 Synthesis of PEI-FI-(PEG-FA) conjugate

The PEG-FA conjugate was synthesized according to a previously reported method.[139] FA (26.48 mg, 60.00 mmol) was first activated with EDC (11.50 mg, 60.00 mmol) and NHS (6.91 mg, 60.00 mmol) in DMSO (4 mL) at room temperature for 3 h. The resulting solution of activated FA was added dropwise into the 4 mL DMSO solution of NH_2-PEG-COOH (60.00 mg, 30.00 mmol) under vigorous magnetic stirring at room temperature for 1 day. The reaction mixture was dialyzed against PBS (3 times, 2 L) for 1.5 days and water (3 times, 2 L) for 1.5 days using a dialysis membrane with MWCO of 1000. This was followed by lyophilization.

PEI-FI-(PEG-FA) conjugates were synthesized taking into account PEG:PEI molar ratios of 1:1. For this, PEI-FI conjugates were first prepared following the same method described in Section 2.2.1. The COOH group of PEG-FA (5.27 mg, 2.16 mmol) was first activated with EDC (4.14 mg, 21.60 mmol) and NHS (2.49 mg, 21.60 mmol) in 5 mL DMSO at room temperature for 3 h. The resulting solution of activated COOH-PEG-FA was added dropwise into PEI-FI in 5 mL DMSO solution under vigorous magnetic stirring at room temperature for 3 days. The reaction mixture

was dialyzed against PBS (3 times, 2L) for 1.5 days and distilled water (3 times, 2L) for 1.5 days through a 10000 MWCO membrane to remove the excess of reactants. This was followed by lyophilization.

2.2.3 Entrapment of Au NPs

Based on a previously reported protocol,[140-141] the PEI-FI-*m*PEG and PEI-FI-(PEG-FA) conjugates synthesized above were used as templates to entrap Au NPs. In each case, molar ratios of 10:1, 25:1 and 50:1 between gold and PEI in each respective conjugate were used to prepare the different Au PENPs. In brief, 200 μL of 48.6 mg/mL $HAuCl_4$ aqueous solution was added to the appropriate amount of conjugates in 10 mL distilled water under vigorous magnetic stirring for 30 min at room temperature. An icy cold $NaBH_4$ solution (1 mL in water/methanol, v/v = 2:1) with 5 molar equivalents of the gold salt was added to the conjugate/gold salt mixture under vigorous stirring. The reaction mixture turned to a deep-red color within a few seconds after adding the $NaBH_4$ solution and the stirring process was continued for 2 h to complete the reaction. The reaction mixture was dialyzed against PBS (3 times, 2L) for 1.5 days and distilled water (3 times, 2L) for 1.5 days through a 10000 MWCO membrane to remove the excess of reactants. This was followed by lyophilization.

2.2.4 Characterization of Au PENPs

^1H NMR spectra of all samples (5 mg sample dissolved in 0.55 mL D_2O or DMSO) were taken at room temperature by using a Bruker 400 MHz Avance II^+ NMR spectrometer. The grafting degree of ligand onto the polymer was determined from the ratio between the peaks through integration and calculation.

UV-Vis spectra of all samples with a concentration of 0.15 mg/mL in distilled water were performed by using a Lambda 2 UV-Vis spectrometer (Perkin-Elmer, USA).

The hydrodynamic size and zeta potential of all the samples were measured by a Zetasizer Nano-ZS (Malvern). The hydrodynamic size of the particles was determined with a scattering angle of 173 ° at 25 ℃. The zeta potential of the particles was measured by using a standard capillary electrophoresis cell in the Zetasizer Nano ZS with a detection angle of 17 ° at 25 ℃. The measurements were performed in triplicates.

2.3 Preparation and characterization of polyplexes

2.3.1 Amplification of pDNA

pDNA encoding for luciferase and enhanced green fluorescent protein (pEGFPLuc, 6.4 kb) with a cytomegalovirus promoter was used. *Escherichia coli* host strain $DH_{5\alpha}$ containing the plasmid was grown overnight in Luria-Broth Base medium with Kanamycin (50 μg/mL). The pDNA was isolated and purified by using the GenElute™ Endotoxin-Free plasmid maxiprep kit. The concentration of pDNA was assessed at 260 nm and 280 nm via a GBC Cintra 40 UV-Vis spectrometer. The pDNA was stored -20 ℃ until further use.

2.3.2 PicoGreen intercalation assay

Polyplexes using a fixed amount of pDNA (0.2 μg) and different concentrations of samples were prepared in a final volume of 100 μL TE buffer (10 mM Tris, 1 mM EDTA, pH 7.5) per well of an opaque 96-well plate. After 20 min incubation at room temperature, 100 μL of PicoGreen® reagent diluted in TE buffer was added to each well and mixed gently. The mixtures were protected from the light and incubated for 5 min at room temperature. Using a microplate reader (model Victor 1420, PerkinElmer), the PicoGreen® fluorescence emission was measured (λ_{ex} = 485 nm, λ_{em} = 535 nm). All experiments were performed in triplicate and the relative fluorescence percentage (%F) was determined using

$$\%F = \frac{F\ complex - F\ blank}{F\ freeDNA - F\ blank} \times 100 \quad (1)$$

The fluorescent value of free DNA was considered as 100%.

2.3.3 Hydrodynamic size and zeta potential measurements of polyplexes

The hydrodynamic size and zeta potential of the polyplexes, which were made of polymer and pDNA at room temperature, were measured by using a Zetasizer Nano-ZS (Malvern). The polyplexes were prepared in water to a final volume of 1 mL, where increasing amounts of conjugates were added to a fixed amount pDNA (4 ug). The samples were then vortexed for 30 s. After incubation for 10 min at room temperature, the measurements were carried out. The measurements were performed in triplicate.

2.4 Gene transfection studies

2.4.1 Cytotoxicity studies

The A2780 human ovarian carcinoma cells were grown in RPMI-1640 medium supplemented with 10% FBS and 1% Antibiotic and Antimycotic (AbAm) solution in a humidified atmosphere at 37 ℃ and 5% CO_2. After a cell confluence of 90% was reached, the A2780 cells were subcultured and seeded into 48-well cell culture plates at 4.5 × 10^4 cells/well using 0.5 mL of cell culture medium. The cells were then incubated overnight in a humidified atmosphere at 37 ℃ and 5% CO_2.

One hour prior to performing the cytotoxicity studies, the spent cell culture medium was replaced with 0.5 mL fresh serum-free medium per well. During this time, the different polyplexes were prepared by adding different concentrations of the polymers (0~3000 nM) to a constant amount of pDNA (the equivalent of 2 μg per well). The resultant mixtures, which were prepared to a final volume of 100 μL, were

vortexed for 30 s and incubated for 10 min at room temperature. Subsequently, the prepared samples were added to each respective well. After 24 h, the cytotoxicity of the samples on the A2780 human ovarian carcinoma cell line was evaluated. This was done by determining the percentage of cell viability using the resazurin reduction assay, which establishes a correlation between the number of viable cells in culture and the cellular metabolic activity. The diluted resazurin reagent (0.1 mg/mL in RPMI medium) was added to every well and the cells were incubated in a humidified atmosphere with 37 ℃ and 5% CO_2. After 3 h incubation, 100 μL of the resultant medium in each well was transferred to opaque-walled 96-well plates and the resorufin fluorescence was measured (λ_{ex} = 530 nm, λ_{em} = 590 nm) using the microplate reader. Untreated cells were considered as having 100% cell viability. All measurements were taken in triplicate.

2.4.2 *In vitro* transfection assay

The A2780 cells, which were grown overnight in RPMI-1640 medium supplemented with 10% FBS and 1% AbAm solution in a humidified atmosphere at 37 ℃ and 5% CO_2, were subcultured and then seeded into 48-well cell culture plates at 4.5 × 10^4 cells/well using 0.5 mL of cell culture medium. The cells were then incubated overnight in a humidified atmosphere at 37 ℃ and 5% CO_2. One hour prior to transfection, the cell culture medium was replaced with 0.5 mL fresh serum-free medium per well. Polyplexes solutions were prepared during this time by mixing a constant amount of pDNA (2 μg pDNA/well) with different vectors at the selected N:P ratio for 30 s and then incubating for 10 min at room temperature. Subsequently, transfection was carried out by adding 100 μL of the prepared polyplexes solutions to the corresponding wells.

After incubating the cells with the polyplexes for 6h, the cell culture medium was replaced with 1 mL serum-containing medium. After further incubation for 48 h, transfection was qualitatively assessed by monitoring the expression of the EGFP gene using an inverted fluorescene microscope (TE2000-E, Nikon Eclipse). The

images of the transfected cells were acquired using the NIS Elements Advanced Research software (version 2.31). The medium was then removed entirely from the cultured cells. PBS was used to rinse the cells. RLB (100 μL) was dispensed into every well and then the plates were placed in the -80 ℃ refrigerator overnight. Following the manufacturer's instructions, the total protein and luciferase activity in the cell lysates were characterized using the bicinchoninic acid (BCA) assay and Promega's luciferase assay, respectively. All samples were run in triplicate. The transfection efficiency was determined quantitatively by evaluating the firefly luciferase expression and denoted as relative light units per mg of protein (RLU/mg protein) ± standard deviation (SD). Non-transfected cells were used as a negative control.

2.4.3 Evaluation of cell-targeting capabilities

To investigate whether the uptake of the Au PENPs was receptor-mediated, the cells were pre-treated with FA to block the FA receptors. This was done by adding 100 μL FA solution (5 μM in serum-free medium) to the A2780 cells which were seeded in 48-well plates 24 h prior to starting this experiment. After incubation for 1 h the cells were then transfected with the vector/pDNA polyplexes under the same conditions as described in Section 2.4.2.

2.5 Gene silencing

2.5.1 Agarose gel electrophoresis retardation assay

Increasing concentrations of polymer and a fixed amount of siRNA (5 pmol) were prepared taking into account different nitrogen:phosphate (N:P) ratios (2.5-30), which corresponds to the molar ratio of amine groups in the polymer to phosphate groups in the siRNA backbone. The mixtures in 6 μL diethylpyrocarbonate (DEPC)-treated water were combined by gentle vortexing and were then incubated for 15 min at room temperature. After incubation, the complexes were analyzed by

agarose gel electrophoresis. For this a 1.0 % (w/v) agarose gel containing ethidium bromide (0.04 μL/mL) was prepared and the samples were then electrophoresed using a current of 120 V for 10 min in TAE buffer solution (40 mM Tris-HCl, 1% v/v acetic acid, 1 mM EDTA). After acquiring images of the gels, the retardation band of each respective complex was assessed.

2.5.2 Hydrodynamic size and zeta potential measurement of complexes

The hydrodynamic size and zeta potential of the complexes, which were made of polymer and siRNA at room temperature, were measured by using a Zetasizer Nano-ZS (Malvern). At first, 900 ng of siRNA was diluted using ultrapure water in each microcentrifuge tube. At selected polymer/siRNA ratios, the complexes were prepared in a total volume of 1 mL and vortexed for 30 s. After incubation for 10 min at room temperature, the measurements were carried out. The measurements were performed in triplicate.

2.5.3 siRNA transfection

Using RPMI-1640 medium supplemented with 10% FBS and 1% AbAm, A2780 cells were seeded in 24-well plates at a density of 4×10^4 cells/well. After 24 h, the spent culture medium was removed and the cells were washed twice with PBS. The Au PENP/siRNA complexes at selected N:P ratios were prepared in DEPC-treated water and were added to the cells in 200 μL fresh serum-free medium. Here, a final volume of 20 μL of the complexes was added per well (each well contained 1.5 μL 10 μM siRNA). After incubation for 4 h at 37 ℃, the cells were washed with PBS twice. RPMI-1640 medium supplemented with 10% FBS and 1% AbAm was added to the cells. After 48 h of incubation, the cells were washed with PBS twice. The cells were then removed from the well surface and then collected by centrifugation at 800 g for 10 min at 4 ℃. The cells were lysed by 20 μL 1 × RLB and then freeze-thawing 3

times. The amount of protein in the cell lysates was quantitated by the BCA assay, with bovine serum albumin (BSA) being used as a standard.

2.5.4 Western blotting

According to the report,[142] an equivalent of 2 μg protein was aliquoted into a microcentrifuge tube and was mixed with loading buffer, using the cell lysates prepared in Section 2.5.3. The prepared mixtures were then heated at 100 ℃ for 8 min. The protein lysates were subsequently assessed by 15% sodium dodecyl sulfate-polyacrylamide gel electrophoresis and transferred onto polyvinylidene fluoride blotting membranes. After blocking the membranes with 5% BSA, they were incubated with the primary anti bcl-2 antibody (1:200 dilution in blocking medium) overnight at 4 ℃. The membranes were then washed 3 times with Tris-buffered saline/tween-20 (TBST) for 10 min each time. Next, the membranes were incubated with horseradish peroxide conjugated secondary antibody (1:1000 dilution in blocking medium) for 2 h at room temperature while shaking. After washing 3 times with TBST at 10 min intervals, the membranes were incubated with the primary anti-tubulin antibody (1:1000 dilution in blocking medium) overnight at 4 ℃. The membranes were subsequently washed 3 times with TBST for 10 min each time. They were then incubated with horseradish peroxide conjugated secondary antibody (1:1000 dilution in blocking medium) for 2 h at room temperature while shaking. This was followed by washing 3 times with TBST for 10 min each time. Finally, the blots were assessed using an Enhanced Chemiluminescence Western Blotting Detection Kit. The protein bands were analyzed using the Image-J software.

In order to determine the gene silencing efficiency of the complexes, the expression of the protein of interest (in this case bcl-2) can be normalized relative to the expression of the internal protein control (in this case tubulin) within the same sample[142]. For this, the normalized intensity of bcl-2 in the sample treated with bcl-2 siRNA can be compared with the normalized intensity of bcl-2 in the sample that underwent no bcl-2 siRNA treatment (see Equation 2). The percentage calculated

using this information corresponds to the expression of the remaining bcl-2 protein in the sample after transfection with the complexes.

$$\frac{Intensity\ of\ bcl\text{-}2\ (sample\ treated\ with\ bcl\text{-}2\ siRNA)/Intensity\ of\ Tubulin\ (sample\ treated\ with\ bcl\text{-}2\ siRNA)}{Intensity\ of\ bcl\text{-}2\ (sample\ treated\ without\ bcl\text{-}2\ siRNA)/Intensity\ of\ Tubulin\ (sample\ treated\ without\ bcl\text{-}2\ siRNA)} \times 100\% \quad (2)$$

2.6 Statistics

One-way ANOVA statistical analyses with Tukey's test were carried out to assess the statistical significance of the experimental data. All results are reported as mean ± SD. 0.05 was selected as the significance level and the data was indicated with (*) for $p < 0.05$, (**) for $p < 0.01$ and (***) for $p < 0.001$, respectively.

CHAPTER 3 – RESULTS AND DISCUSSION

CHAPTER 3 – RESULTS AND DISCUSSION

3.1 Preparation of Au PENPs

3.1.1 Synthesis and characterization of PEI-FI-*m*PEG conjugate

In this work, a novel non-viral vector for nucleic acid delivery was prepared. PEI, which is amongst the typically used polymeric gene vectors,[143] was selected as the polymer backbone in this study, as it possesses a large number of amine groups that are able to condense nucleic acid, buffer and rupture the acidic environment of endolysosomes, resulting in the superior transfection efficiency.[144] The FI moiety, which is generally used as a fluorescent probe, was covalently conjugated onto the PEI backbone in order to trace the intracellular uptake of PEI. The *m*PEG moiety was further coupled to the PEI backbone by covalent attachment so as to increase the hydrophilicity and reduce the cytotoxicity of the prepared conjugate.

The first step in the overall synthesis of the PEI-FI-*m*PEG conjugate involved the preparation of the PEI-FI conjugate using PEI and FI (see synthesis process depicted in Figure 7). The ^{1}H NMR spectra of PEI and FI are shown in Figure 33 and Figure 34 respectively in ANNEX I. In the ^{1}H NMR spectrum acquired for the PEI-FI conjugate in D_2O (Figure 8), the chemical shift between 2.0 and 3.4 ppm was assigned to the characteristic proton peaks of PEI containing eight broad, overlapping peaks, while the chemical shift between 6.5 and 8.0 ppm was assigned to the characteristic proton peaks of the FI moiety.[144-146] Because free FI moieties were cleared out from the reaction mixture during dialysis, the FI peaks in the ^{1}H NMR spectrum of PEI-FI may be attributed to the FI moieties that were covalently attached to the PEI backbone. Based on the integration of the relevant peaks, the ratio of FI moieties attached onto the PEI backbone was estimated to be 6: 1.

In the second step, the PEI-FI-*m*PEG conjugate was synthesized through conjugation of *m*PEG to the above prepared PEI-FI conjugate. The ^{1}H NMR spectrum

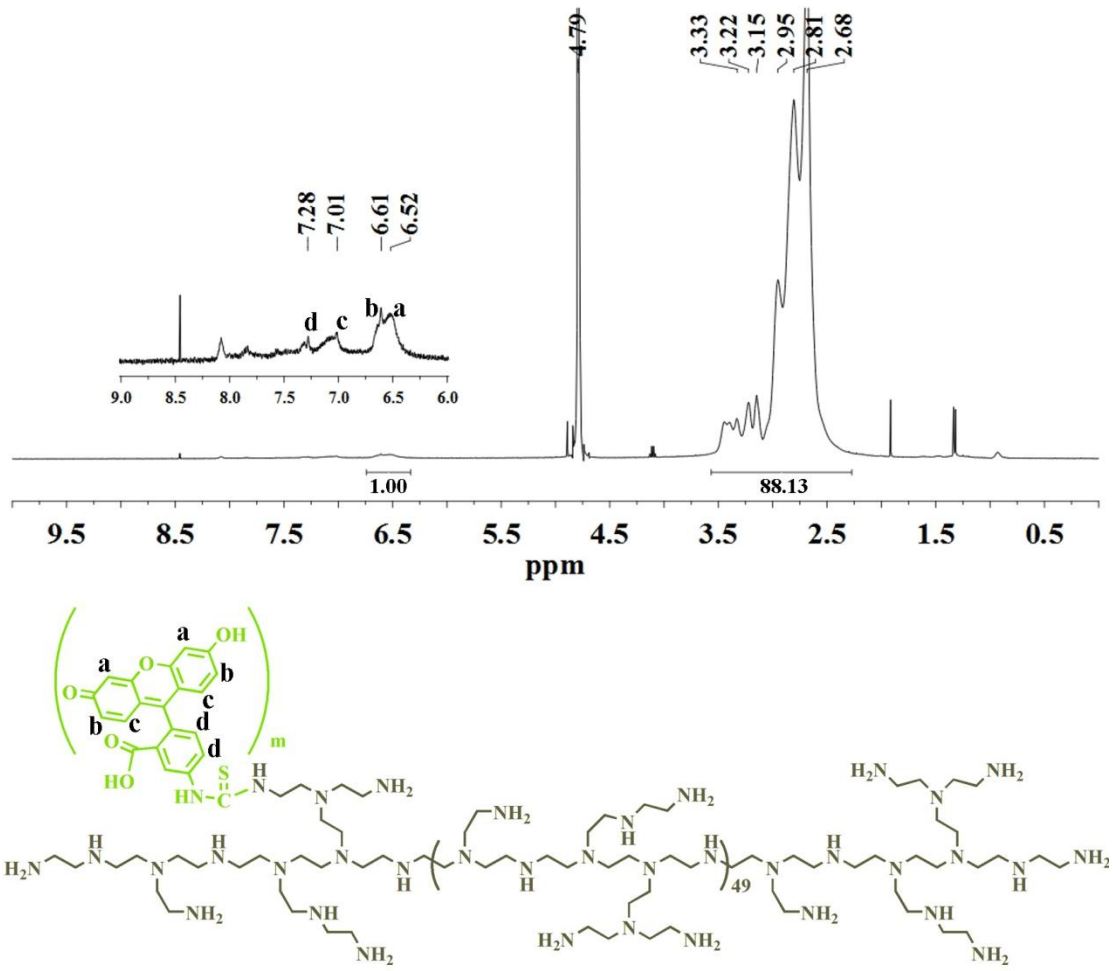

Figure 8 ^{1}H NMR spectrum of PEI-FI in D_2O. The chemical shift at 4.79 ppm corresponds to the D_2O solvent. The letters in the PEI-FI conjugate structure correspond to the peaks identified in ^{1}H NMR spectrum.

of *m*PEG is presented in ANNEX I (Figure 35). In the ^{1}H NMR spectrum of PEI-FI-*m*PEG in D_2O shown in Figure 9, the characteristic peak of the *m*PEG methylene protons can be seen at 3.7 ppm. This chemical shift represents only the *m*PEG moieties that were covalently attached to PEI-FI, since any free mPEG moieties were cleared out from the reaction mixture during dialysis. Based on the integration of the relevant peaks, the ratio of PEI: FI: *m*PEG was estimated to be 1:6:1.

UV-Vis spectroscopy was used for further characterization of the synthesized conjugates. From the UV-Vis spectra acquired for PEI-FI and PEI-FI-*m*PEG (Figure 10), absorbance peak at 495 nm is evident, which corresponds to the characteristic absorption of FI.[147] This data combined with the NMR analysis above, indicated the successful synthesis of the PEI-FI-*m*PEG conjugate.

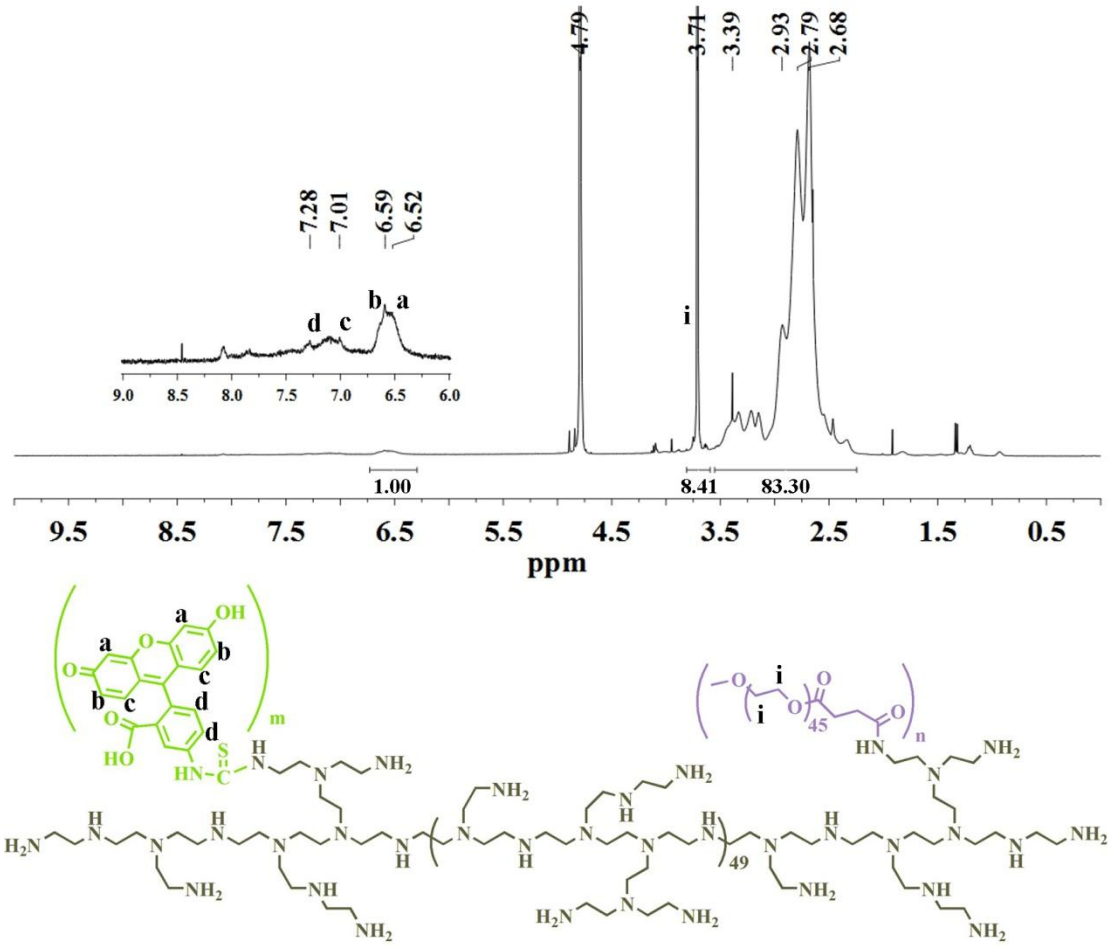

Figure 9 ^{1}H NMR spectrum of PEI-FI-*m*PEG in D_2O. The chemical shift at 4.79 ppm corresponds to the D_2O solvent. The letters in the PEI-FI-*m*PEG conjugate structure correspond to the peaks identified in ^{1}H NMR spectrum.

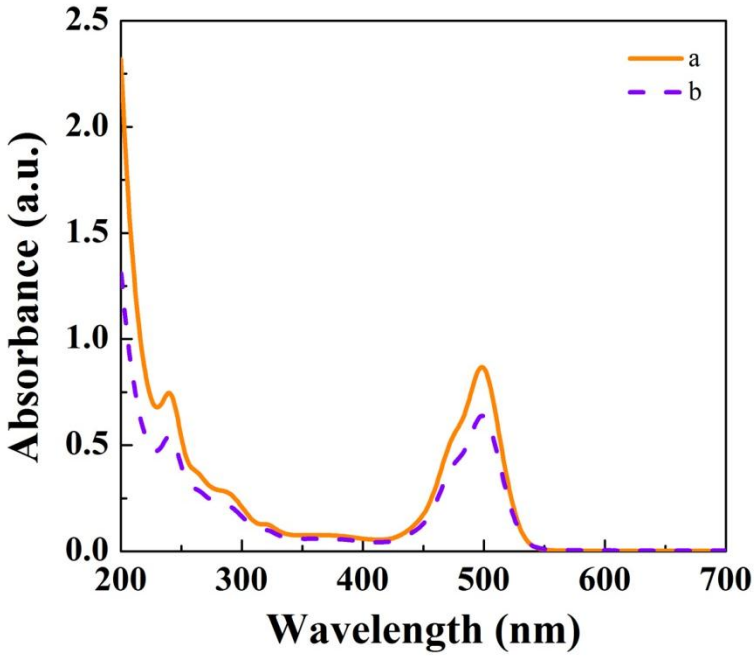

Figure 10 UV-Vis spectra of the PEI-FI (a) and the PEI-FI-*m*PEG (b) conjugates. Each sample was prepared in distilled water at a concentration of 0.15 mg/mL.

3.1.2 Synthesis and characterization of PEI-FI-(PEG-FA) conjugate

For the purpose of targeted gene therapy applications, PEI-FI-(PEG-FA) conjugates were also prepared. In addition to PEI and FI, the properties of which were described in Section 3.1.1, FA targeting moieties were conjugated onto the PEI polymer. The FA moiety was used as the targeting motif to target nucleic acid delivery to cancer cells overexpressing FA receptors, which are receptors known to be expressed in most human carcinoma cell lines.[148] The PEG moiety, which served as a spacer, was covalently linked between PEI and FA. This was done not only to decrease the hydrophobicity and cytotoxicity of the conjugate, but also to increase the targeting probability of FA in each of the prepared conjugate systems.

For the synthesis of the PEI-FI-(PEG-FA) conjugate, the PEG-FA was first prepared. This was achieved through conjugation of activated FA onto the terminal amine group of PEG (see synthesis process depicted in Figure 11). The ^{1}H NMR spectra of PEG and FA are shown in Figure 36 and Figure 37 respectively in ANNEX I. In the ^{1}H NMR spectrum acquired for PEG-FA in D_2O (Figure 12), the characteristic proton peak at 3.7 ppm was assigned to the PEG moiety, while the characteristic proton peaks at 2.0, 6.8, 7.7 and 8.8 ppm were assigned to the attached FA moiety.[35] Because free FA moieties were cleared out from the reaction mixture during dialysis, the presence of the characteristic FA and PEG peaks in the ^{1}H NMR spectrum are indicative of the effective covalent attachment of FA to PEG. Based on the integration of the relevant peaks, the ratio of PEG:FA was estimated to be 1:1.

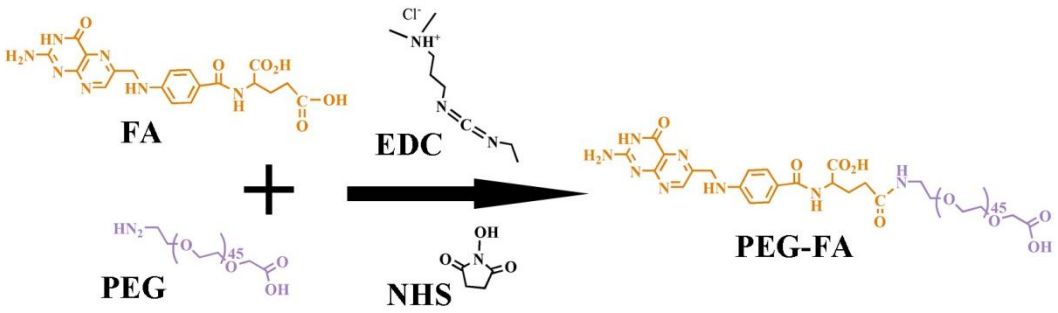

Figure 11 Synthesis process of the PEG-FA conjugate.

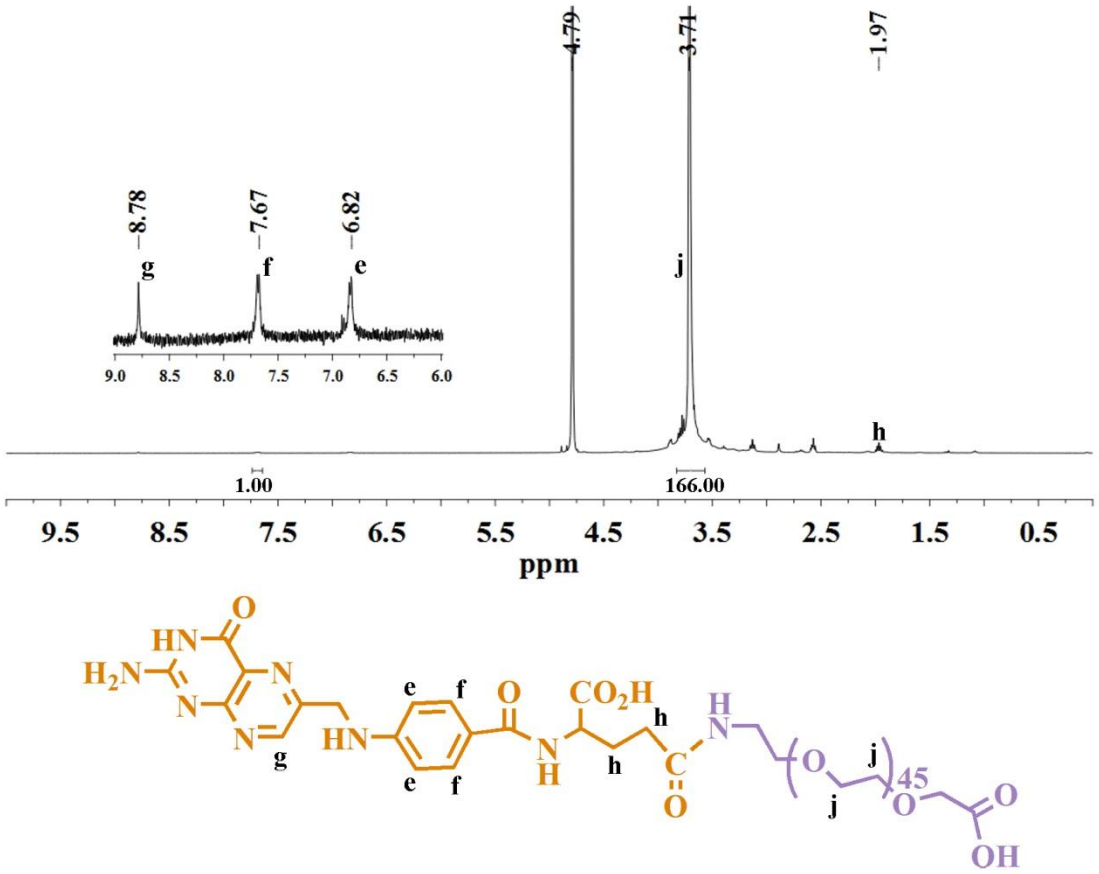

Figure 12 ^{1}H NMR spectrum of PEG-FA in D_2O. The chemical shift at 4.79 ppm corresponds to the D_2O solvent. The letters in the PEG-FA conjugate structure correspond to the peaks identified in ^{1}H NMR spectrum.

In the next step, the synthesis of the final PEI-FI-(PEG-FA) conjugate involved conjugation of PEG-FA onto the terminal amine group of PEI-FI. Figure 13 showed the ^{1}H NMR spectrum and peak assignment of the final PEI-FI-(PEG-FA) conjugate in D_2O. The characteristic proton peaks at 2.0-3.4, 6.5, 6.6, 7.1 and 7.3 ppm were assigned to the PEI-FI moiety, while the characteristic proton peaks at 1.9, 3.7, 6.9, 7.7 and 8.7 ppm were assigned to the PEG-FA moiety. Combined, the presence of these peaks was indicative of the successful synthesis of PEI-FI-(PEG-FA). Furthermore, based on the identification of the characteristic peaks in the conjugate and the integration of the relevant peaks, the ratio of PEI:FI:PEG:FA was estimated to be 1:7:1:1.

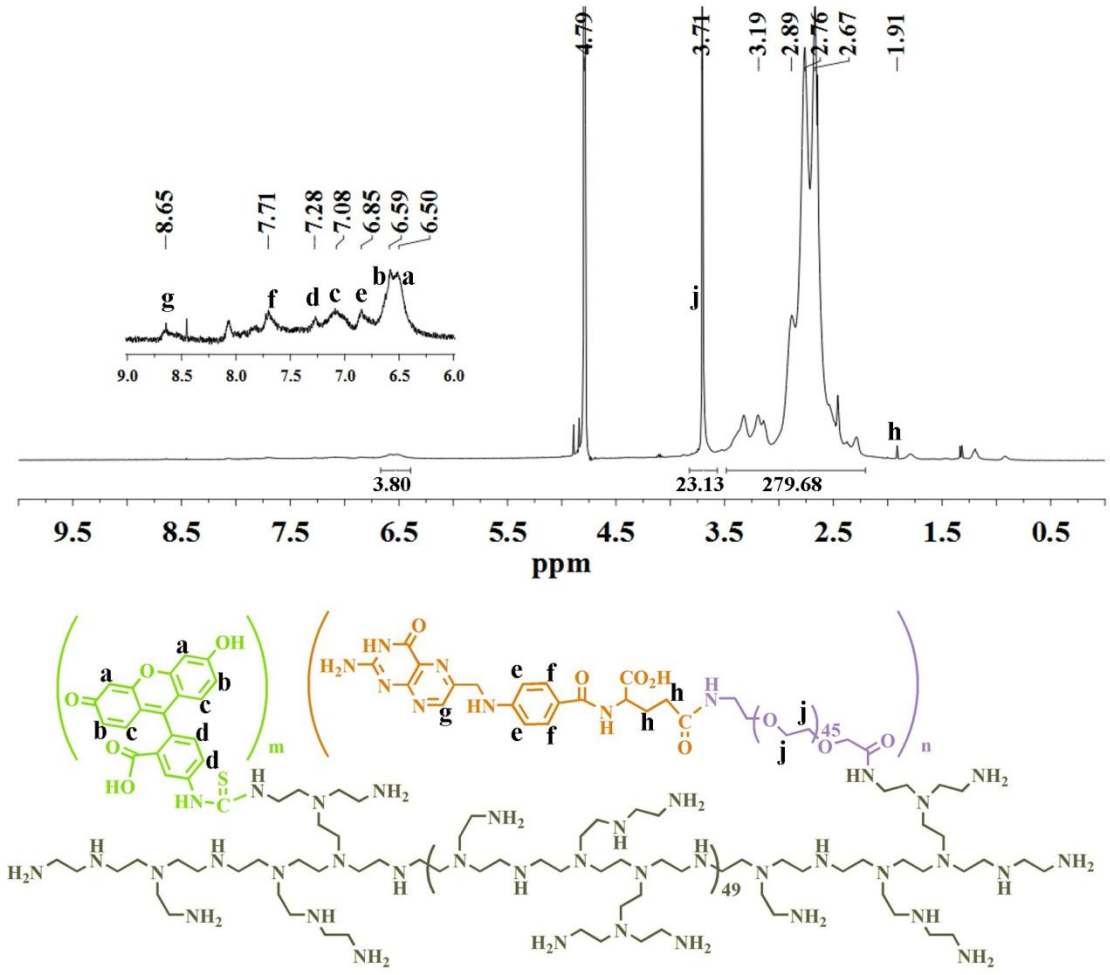

Figure 13 ^{1}H NMR spectrum of PEI-FI-(PEG-FA) in D_2O. The chemical shift at 4.79 ppm corresponds to the D_2O solvent. The letters in the PEI-FI-(PEG-FA) conjugate structure correspond to the peaks identified in ^{1}H NMR spectrum.

UV-Vis spectroscopy was further used to characterize the synthesized PEI-FI-(PEG-FA) conjugate (Figure 14). For comparison purposes, the UV-Vis spectra of PEI-FI and PEG-FA were also included. Both PEI-FI and PEI-FI-(PEG-FA) were observed to display an absorbance peak at 495 nm, which corresponds to the characteristic absorption of FI.[147] Relative to PEI-FI, the conjugates possessing FA showed absorbance peaks at 280 nm and 360 nm, which correspond to the characteristic absorption of FA.[149-150] Combined, the UV-Vis and NMR data indicated the successful synthesis of the PEI-FI-(PEG-FA) conjugate.

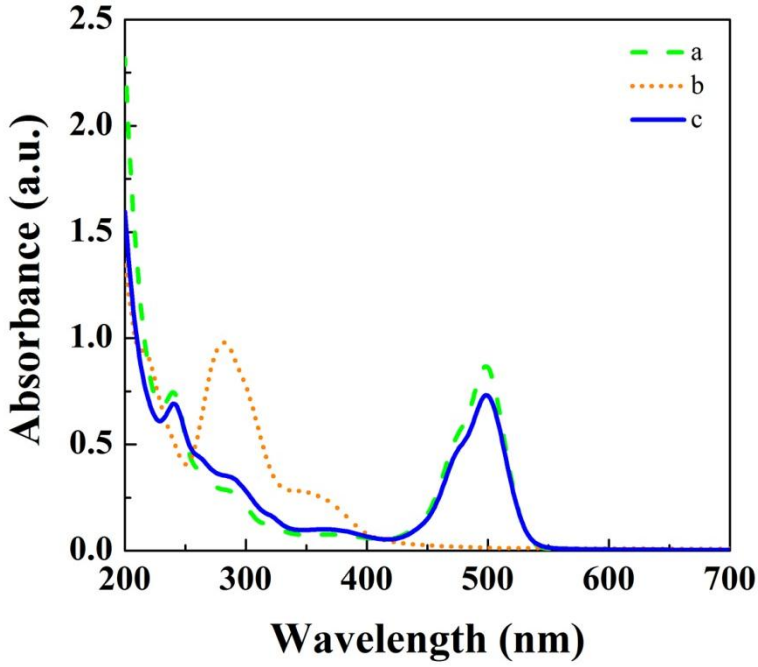

Figure 14 UV-Vis spectra of the PEI-FI (a), PEG-FA (b) and PEI-FI-(PEG-FA) (c) conjugates. Each sample was prepared in distilled water at a concentration of 0.15 mg/mL.

3.1.3 Preparation and characterization of Au PENPs

Currently, Au NPs form the focus of nucleic acid delivery studies owing to their stability and affinity for nucleic acid. By optimizing several factors, such as size, surface coatings and surface charge, Au NPs have been used for enhancing transfection efficiency and reducing cytotoxicity.[151] In this work, the synthesized PEI-FI-*m*PEG and PEI-FI-(PEG-FA) conjugates served as templates to entrap Au NPs (see Figure 15). Au atom:PEI molar ratios of 10:1, 25:1 and 50:1 were used to prepare the different Au PENPs.

When in solution, the produced Au PENPs did not aggregate. Relative to the respective PEI-FI-*m*PEG and PEI-FI-(PEG-FA) conjugates, the corresponding Au PENPs were also observed to be red in color (see Figure 16) thereby providing evidence for the formation of Au PENPs. Furthermore, this red color was observed to become more prominent with an increase in the molar ratio of Au atom:PEI from 10:1 to 50:1.

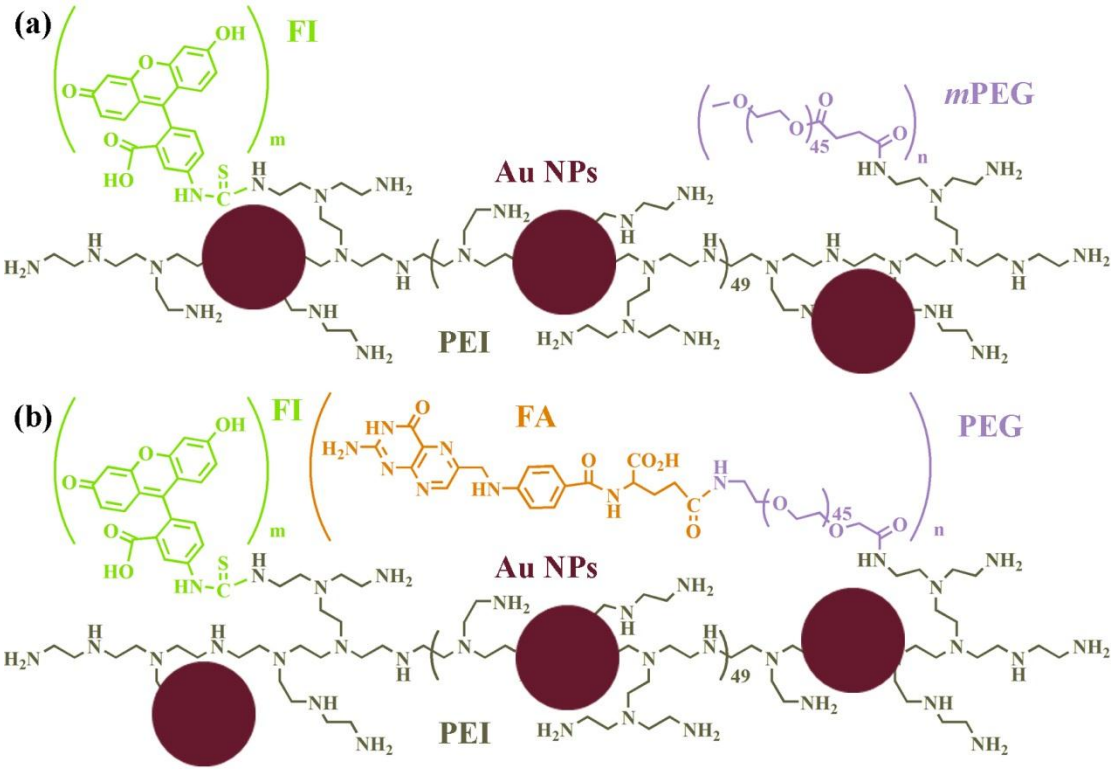

Figure 15 Schematic illustration of the structure of the synthesized Au PENPs prepared using PEI-FI-*m*PEG (a) and PEI-FI-(PEG-FA) (b).

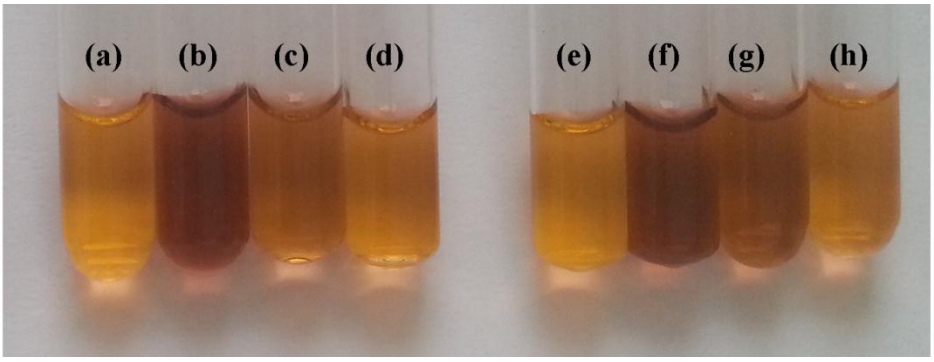

Figure 16 Photographs of PEI-FI-*m*PEG (a), $(Au^0)_{50}$-PEI-FI-*m*PEG (b), $(Au^0)_{25}$-PEI-FI-*m*PEG (c), $(Au^0)_{10}$-PEI-FI-*m*PEG (d), PEI-FI-(PEG-FA) (e), $(Au^0)_{50}$-PEI-FI-(PEG-FA) (f), $(Au^0)_{25}$-PEI-FI-(PEG-FA) (g) and $(Au^0)_{10}$-PEI-FI-(PEG-FA) (h) dispersed in ultrapure water. The concentration of each sample was 1 mg/mL.

UV-Vis spectroscopy was used to characterize the Au PENPs that were synthesized. The spectra for the Au PENPs produced using either the PEI-FI-*m*PEG or the PEI-FI-(PEG-FA) conjugates as templates are shown in Figure 17 and Figure 18, respectively. For all the Au PENPs, an absorbance peak at 495 nm was apparent in the spectrum indicating the characteristic absorption of FI. In the case of all the

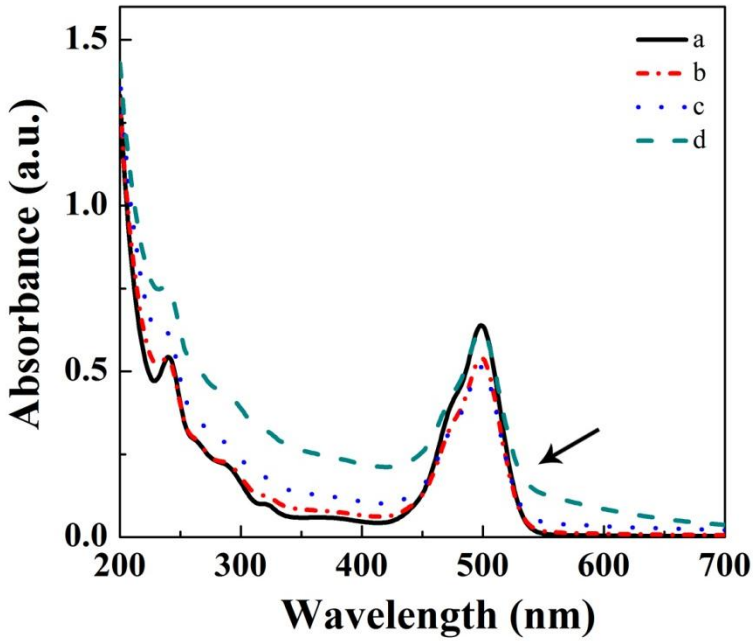

Figure 17 UV-Vis spectra of PEI-FI-*m*PEG (a), $(Au^0)_{10}$-PEI-FI-*m*PEG (b), $(Au^0)_{25}$-PEI-FI-*m*PEG (c) and $(Au^0)_{50}$-PEI-FI-*m*PEG (d). Each sample was prepared in distilled water at a concentration of 0.15 mg/mL.

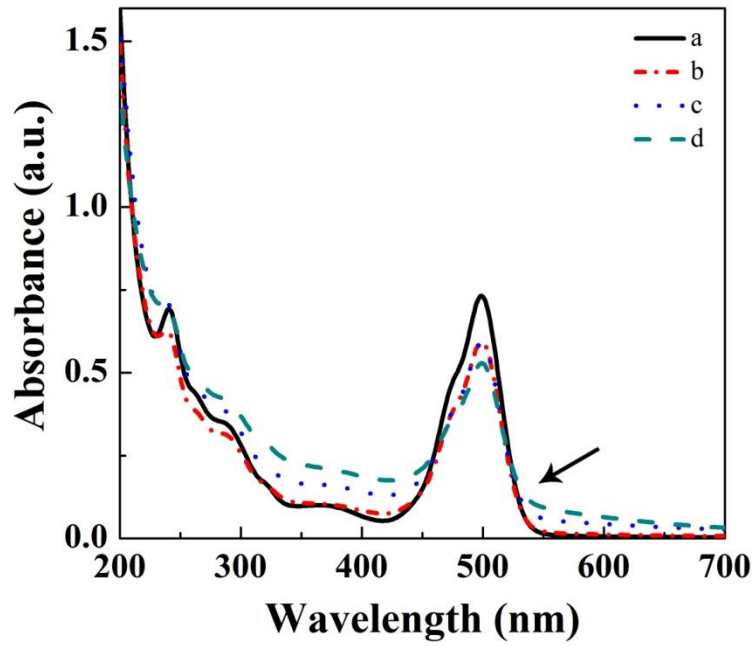

Figure 18 UV-Vis spectra of PEI-FI-(PEG-FA) (a), $(Au^0)_{10}$-PEI-FI-(PEG-FA) (b), $(Au^0)_{25}$-PEI-FI-(PEG-FA) (c) and $(Au^0)_{50}$-PEI-FI-(PEG-FA) (d). Each sample was prepared in distilled water at a concentration of 0.15 mg/mL.

FA-containing Au PENPs (see Figure 18), the presence of FA was confirmed due to the presence of the absorbance peaks at 280 nm and 360 nm which correspond to the characteristic absorption of FA.[149-150] The existence of Au NPs in the different Au PENPs however was difficult to confirm through UV-Vis as the absorption of the FI moieties overlapped the surface plasmon resonance peak of the Au NPs at 520 nm. This effect was enhanced when the amount of Au NPs entrapped within the different conjugates was extremely low. However, the broad shoulder evident at 550 nm in the spectra acquired for each Au NP-containing sample provides an indication of the existence of the Au NPs.[152] This shoulder was observed to become more prominent as the molar ratio of Au atom:PEI increased. In contrast, samples without Au NPs don't show this specific absorbance feature.

3.2 Characterization of polyplexes formed by conjugates and Au PENPs with pDNA

3.2.1 PicoGreen intercalation assay

In order to ensure cell entry, compaction of pDNA by the vector is crucial. Thus, to assess the pDNA compaction capabilities of the different vectors that were synthesized, the PicoGreen® intercalation assay was used. PicoGreen®, which is a high affinity intercalator, is practically non-fluorescent in its free form and becomes highly fluorescent after binding free double stranded DNA.[153]

Figure 19 shows the PicoGreen® intercalation assay data obtained for each pDNA/conjugate and pDNA/Au PENP polyplexes. The fluorescent signal acquired for free pDNA (N:P ratio of 0) indicates that PicoGreen® is completely bound to it. The relative fluorescence intensity recorded for each pDNA/conjugate and pDNA/Au PENP polyplexes was then observed to decrease with an increase in the concentration of the vector under investigation (i.e., with increasing N:P ratios), thereby indicating the ability of each vector to compact pDNA. Moreover, complete pDNA packaging

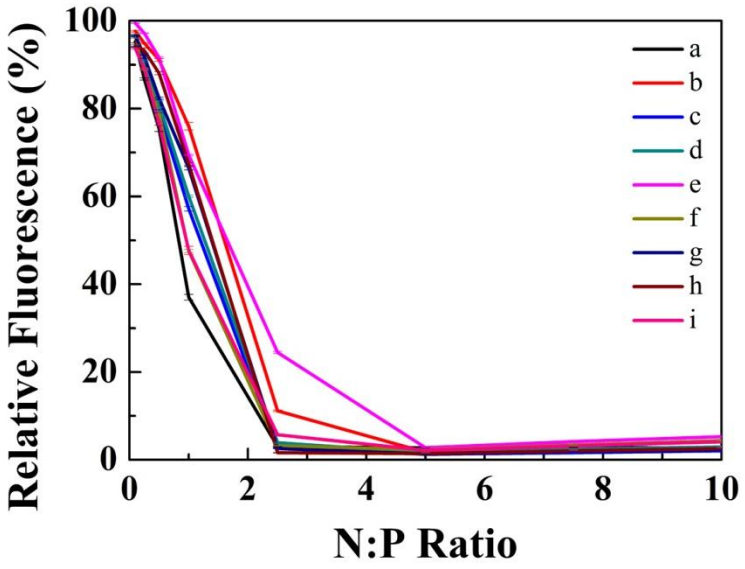

Figure 19 PicoGreen® intercalation assay of pDNA bound to either PEI (a), PEI-FI-*m*PEG (b), $(Au^0)_{10}$-PEI-FI-*m*PEG (c), $(Au^0)_{25}$-PEI-FI-*m*PEG (d), $(Au^0)_{50}$-PEI-FI-*m*PEG (e), PEI-FI-(PEG-FA) (f), $(Au^0)_{10}$-PEI-FI-(PEG-FA) (g), $(Au^0)_{25}$-PEI-FI-(PEG-FA) (h) or $(Au^0)_{50}$-PEI-FI-(PEG-FA) (i). N:P ratios ranging from 0 (pDNA only) to 10 were assessed. The results are reported as the relative percentage of PicoGreen fluorescence, in which 100% intensity corresponds to zero concentration of polyplexes (only pDNA). All results were expressed as the mean ± SD, n = 3.

was achieved by each vector when using a N:P ratio of 2.5 or more, relealing that pDNA is no longer accessible to this intercalating fluorochromes.[29, 154-156] Thus N:P ratos of 5 were selected to further study.

3.2.2 Hydrodynamic size and zeta potential measurements

The hydrodynamic size and zeta potential of pDNA/vector ploylexes are known to be critical factors that influence gene delivery. For this purpose, DLS and zeta potential measurements can be acquired to evaluate the size and zeta potential of any polyplexes of interest.

Figure 20 (also see ANNEX I, Table 1) shows the hydrodynamic size of the different pDNA/vector polyplexes that were prepared using the selected N:P ratio. The polyplexes formed between pDNA with vectors based on PEI-FI-*m*PEG showed a relatively larger hydrodynamic radius (203~360 nm), while the polyplexes formed between pDNA with vectors based on PEI-FI-(PEG-FA) showed a relatively smaller hydrodynamic radius(138~171 nm), which is presumably due to the influence of the

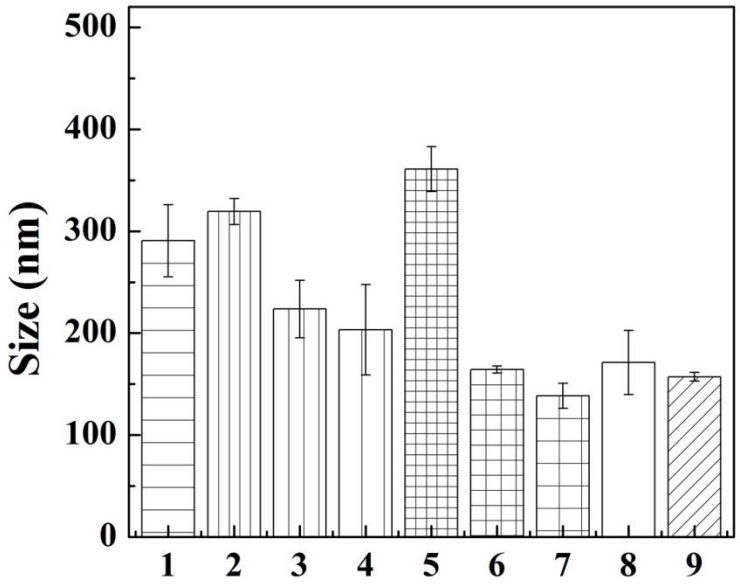

Figure 20 Hydrodynamic size of the polyplexes prepared by complexing pDNA with PEI (1), PEI-FI-*m*PEG (2), $(Au^0)_{10}$-PEI-FI-*m*PEG (3), $(Au^0)_{25}$-PEI-FI-*m*PEG (4), $(Au^0)_{50}$-PEI-FI-*m*PEG (5), PEI-FI-(PEG-FA) (6), $(Au^0)_{10}$-PEI-FI-(PEG-FA) (7), $(Au^0)_{25}$-PEI-FI-(PEG-FA) (8) and $(Au^0)_{50}$-PEI-FI-(PEG-FA) (9). All results were expressed as the mean ± SD, n =3.

FA structure or property. These polyplexes were in nano-scale, which indicated that there was no aggregate in solution. The hydrodynamic radius of them were similar with that of pDNA/PEI polyplexes, so they might be uptaken by cells. There is the no significant difference between groups (ANNEX I, Table 1).

The zeta potentials of the different pDNA/vector polyplexes, which were prepared using the selected N:P ratio, are shown in Figure 21 (also see ANNEX I, Table 1). For all the polyplexes of the synthesized vectors, positive zeta potential values of 40~45 mV were recorded. Since these polyplexes were positively charged, they were likely to establish electrostatic interactions with the negatively charged cell membrane thereby promoting pDNA delivery. Furthermore, the steric shielding effect of PEGylation, which is that the zeta potential decreased with the number of the PEG moieties grafted at the conjugate surface, was one of the most important approaches to control surface charge.[80, 157] But in this case, since the number of the PEG moieties attached was less, the zeta potential values acquired for the different polyplexes did not indicate the steric shielding effect of PEGylation, but showed the reverse phenomenon with no significance difference (as can be seen by the zeta potential values recorded in Table 1 in ANNEX I).

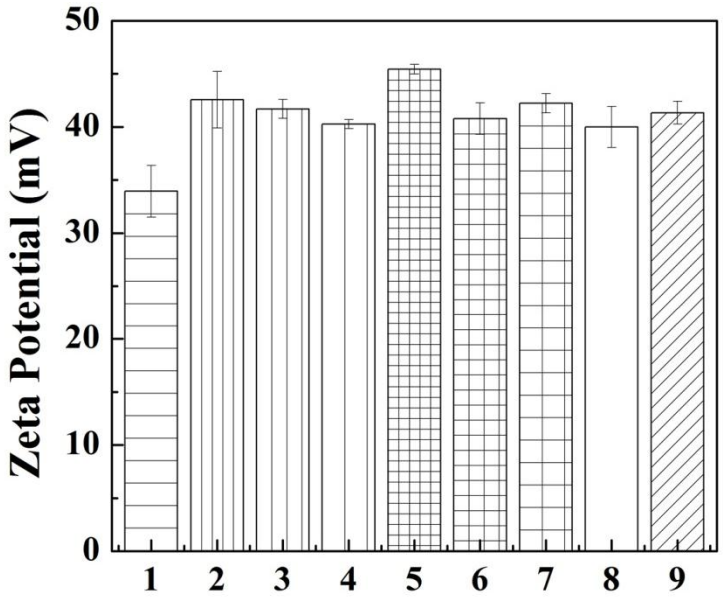

Figure 21 Zeta potential of the polyplexes prepared by complexing pDNA with PEI (1), PEI-FI-*m*PEG (2), $(Au^0)_{10}$-PEI-FI-*m*PEG (3), $(Au^0)_{25}$-PEI-FI-*m*PEG (4), $(Au^0)_{50}$-PEI-FI-*m*PEG (5), PEI-FI-(PEG-FA) (6), $(Au^0)_{10}$-PEI-FI-(PEG-FA) (7), $(Au^0)_{25}$-PEI-FI-(PEG-FA) (8) and $(Au^0)_{50}$-PEI-FI-(PEG-FA) (9). All results were expressed as the mean ± SD, n =3.

3.3 Gene delivery

3.3.1 Cytotoxicity studies

Prior to assessing the nucleic acid delivery applications of the synthesized vectors, their cytotoxicity on A2780 human ovarian carcinoma cells was tested using the resazurin cell viability assay (see Figure 22 and Figure 23). Broadly speaking, the viability was observed to decrease, when treating the cells with increasing concentrations of each vector. Compared to PEI, all the vectors were less toxic particularly when using concentrations of 200 nM or higher. Moreover, the cell viability was noticeably higher upon treatment with 500 and 1000 nM concentrations of the PEG-containing vectors relative to treatment with the equivalent concentrations of PEI (p<0.001). This may be due to the fact that PEG surface modification of the PEI backbone increases the hydrophilicity of the polyplexes, which alleviates the strong electrostatic interaction between the vector and the cell surface, consequently resulting in a reduced cytotoxic effect.[158]

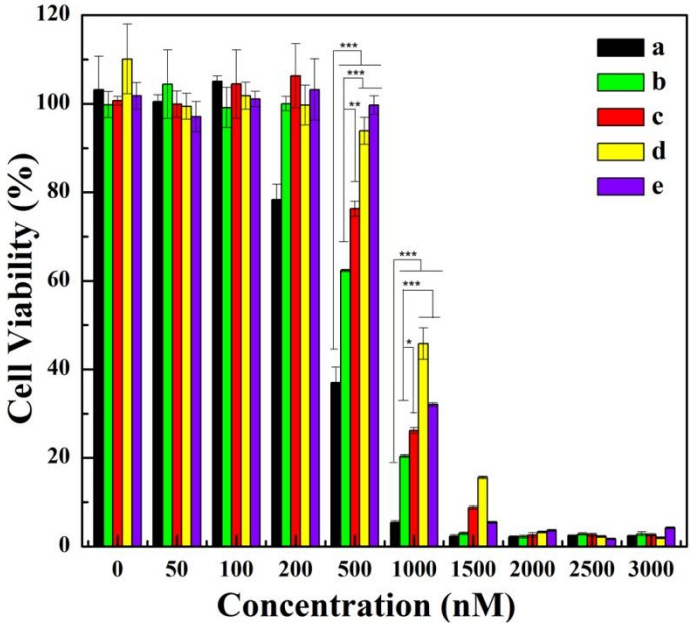

Figure 22 Resazurin cell viability assay on A2780 human ovarian carcinoma cells after treatment with PEI (a), PEI-FI-*m*PEG (b), $(Au^0)_{10}$-PEI-FI-*m*PEG (c), $(Au^0)_{25}$-PEI-FI-*m*PEG (d) and $(Au^0)_{50}$-PEI-FI-*m*PEG (e). In each case increasing concentrations of each vector were used to treat the cells. All results were expressed as the mean ± SD, n =3.

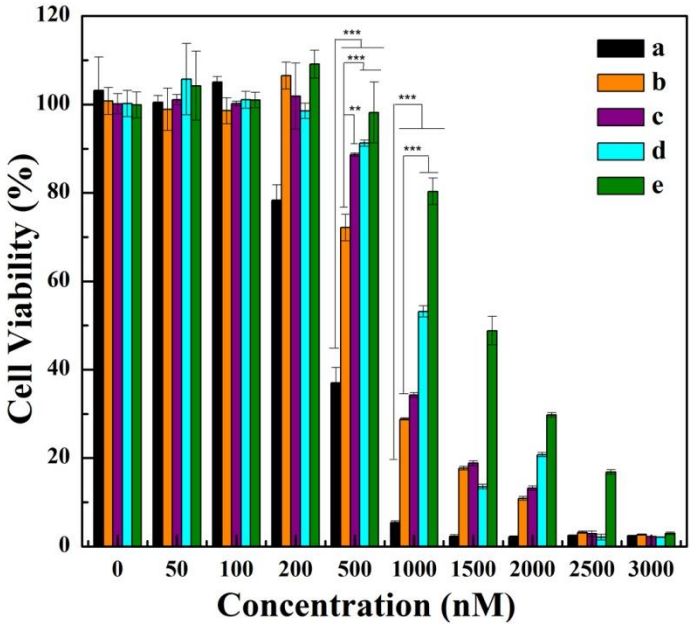

Figure 23 Resazurin cell viability assay on A2780 human ovarian carcinoma cells after treatment with PEI (a), PEI-FI-(PEI-FA) (b), $(Au^0)_{10}$-PEI-FI-(PEI-FA) (c), $(Au^0)_{25}$-PEI-FI-(PEI-FA) (d) and $(Au^0)_{50}$-PEI-FI-(PEI-FA) (e). In each case increasing concentrations of each vector were used to treat the cells. All results were expressed as the mean ± SD, n =3.

Further comparison of the Au NP-free and Au NP-containing conjugate systems (see Figure 22 and Figure 23) also revealed a difference in cytotoxic effects. Overall, cell viability was notably increased for the cells undergoing treatment with the Au NPs-containing conjugate systems relative to their Au-free counterparts. Thus, entrapment of Au NPs seems to be good for reducing cytotoxicity. This may be explained by the fact that the amine group of PEI, which contributes to the cytotoxic effects of the polymer, behave as reductant and stabilizer, as well as bind colloidal Au tightly via the available electron lone pairs.[159-161] This entrapment of the Au NPs leads to a decrease in the number of free amines, resulting in lower cytotoxicity.

3.3.2 *In vitro* transfection assay

The gene transfection efficiency of the Au PENP/pDNA polyplexes was investigated through the delivery of pEGFPLuc into A2780 human ovarian carcinoma cells *in vitro*. For this, pEGFPLuc expression was assessed 48 h post-transfection by monitoring the fluorescent and luminescent properties of EGFP and Luc, respectively.

In the first set of the gene delivery studies, the cells were assayed for expression of the Luc reporter gene. The luciferase activity, which was normalized for the protein content, is shown as RLU in Figure 24. Compared to PEI, the PEI-FI-*m*PEG conjugate demonstrated an enhanced transfection efficiency. In contrast, relative to PEI-FI-*m*PEG, a reduction in transfection efficiency was observed when using the corresponding Au PENP vectors ($p<0.01$).Compared to PEI, the PEI-FI-(PEG-FA) and the corresponding Au PENP vectors demonstrated an reduced transfection efficiency without the significant difference.

The gene delivery ability of the different vector systems was then qualitatively evaluated by visualization of EGF expression using fluorescence microscopy. Figure 25 shows the fluorescence microscopy images that were acquired. As can be seen by the expression of EGFP in the fluorescence microscopy images, all the synthesized conjugates and Au PENPs were able to successfully transfect the A2780 cells. Moreover, the transfection efficiency observed for each vector was in accordance with the observations recorded through quantitative analysis of the Luc reporter gene.

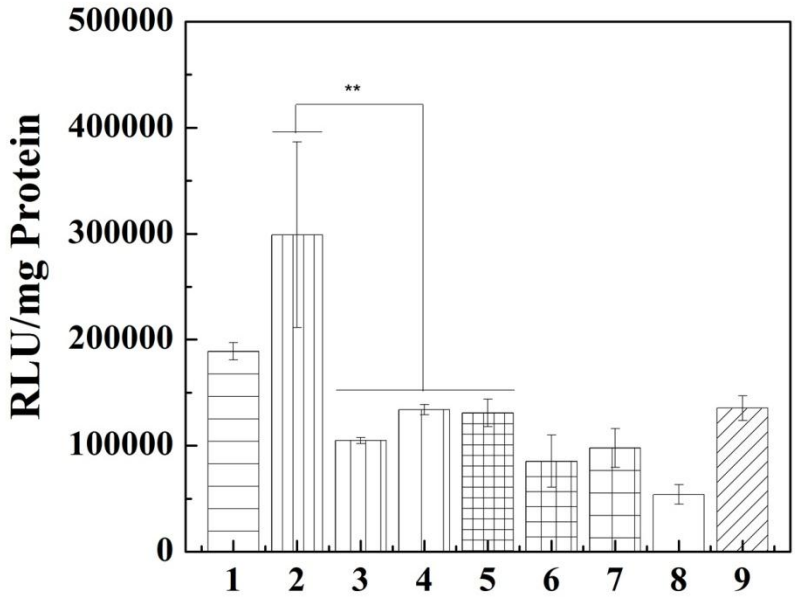

Figure 24 *In vitro* Luc gene expression in A2780 human ovarian carcinoma 48 h post-transfection. Cells were treated with polyplexes prepared using pDNA complexed with PEI (1), PEI-FI-*m*PEG (2), $(Au^0)_{10}$-PEI-FI-*m*PEG (3), $(Au^0)_{25}$-PEI-FI-*m*PEG (4), $(Au^0)_{50}$-PEI-FI-*m*PEG (5), PEI-FI-(PEG-FA) (6), $(Au^0)_{10}$-PEI-FI-(PEG-FA) (7), $(Au^0)_{25}$-PEI-FI-(PEG-FA) (8) ,$(Au^0)_{50}$-PEI-FI-(PEG-FA) (9). All results were expressed as the mean ± SD, n = 3.

Combined, this data indicates that the positively charged polyplexes, in which the negatively charged nucleic acid was neutralized by the synthesized vector (see Section 3.2.2), interacted with the negatively charged cell membrane and was internalized into the cell. Overall, the efficiency of cell transfection was dependent on the charge properties of the vector used. The more positively charged the vector making up the polyplexes, the better the transfection efficiency. In the case of the Au PENPs, the molar ratio of Au atom:PEI was found to influence transfection efficiency, with the Au atom:PEI molar ratio of 50:1 demonstrating the best results. This may be due to the reduction of interior space in the polymer and the decrease in the number of amines in the conjugates after entrapment of the Au NPs. Finally, the noticeable difference in transfection efficiency between the PEI-FI-*m*PEG and the PEI-FI-(PEG-FA) based vector systems may be attributed to the FA moiety. The presence of this moiety in the vector system may have an influence on the structure of the conjugate, resulting in lower transfection efficiency.

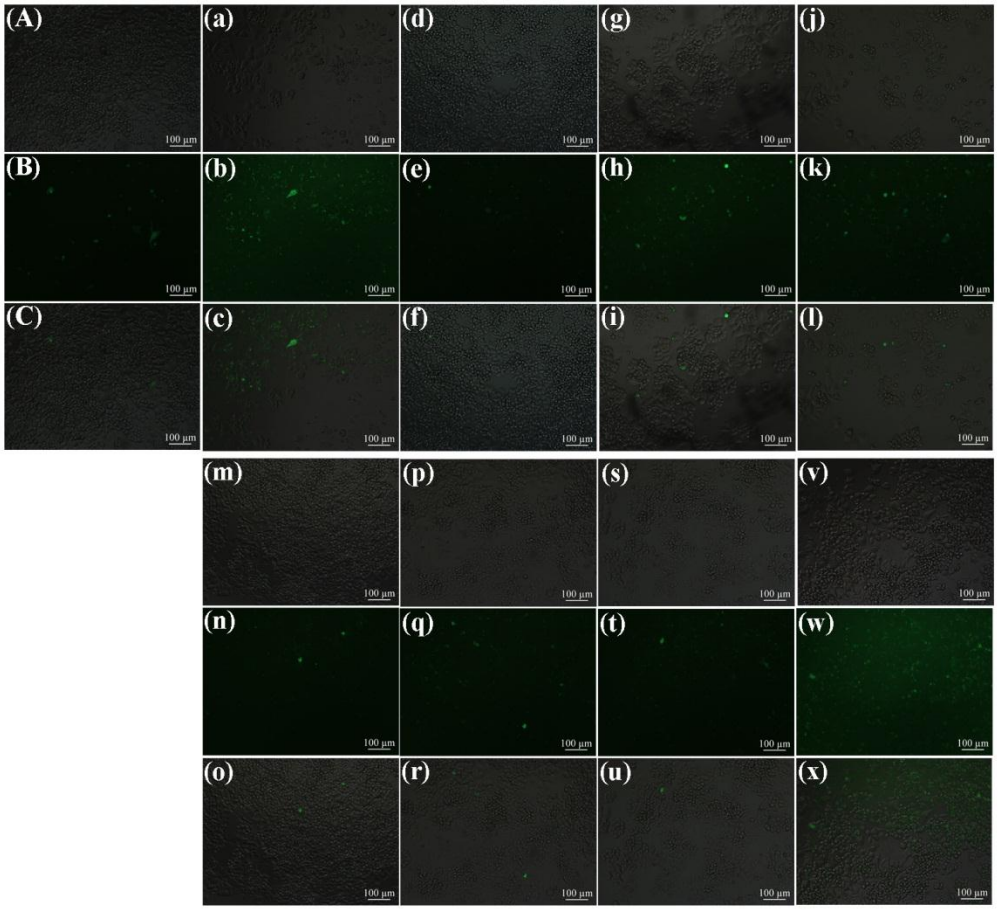

Figure 25 EGFP expression in A2780 human ovarian carcinoma 48 h post-transfection. Cells were treated with polyplexes prepared using pDNA complexed with PEI (A-C), PEI-FI-*m*PEG (a-c), $(Au^0)_{10}$-PEI-FI-*m*PEG (d-f), $(Au^0)_{25}$-PEI-FI-*m*PEG (g-i), $(Au^0)_{50}$-PEI-FI-*m*PEG (j-l), PEI-FI-(PEG-FA) (m-o), $(Au^0)_{10}$-PEI-FI-(PEG-FA) (p-r), $(Au^0)_{25}$-PEI-FI-(PEG-FA) (s-u) ,$(Au^0)_{50}$-PEI-FI-(PEG-FA) (y-x). Bright field images (first and fourth row), fluorescence microscopy images (second and fifth row) and the corresponding merged micrographs (third and sixth row) are shown.

3.3.3 Evaluation of cell-targeting capabilities

To achieve targeted gene delivery to cancer cells overexpressing FA receptors on their membrane surface, the FA moiety was selected as the targeting ligand to be conjugated onto PEI. Thus, the high affinity of FA receptors for FA is expected to play a role in specifically binding and internalizing the PEI-FI-(PEG-FA) conjugate and its respective Au PENPs. In order to evaluate this and determine whether the uptake of these vectors is receptor-mediated, gene transfection studies using A2780 human ovarian carcinoma cells that overexpress the FA receptor were performed. Here, the

cells were first pre-treated with FA for 1 h to block the FA receptors and then transfected with the different pEGFPLuc/vector polyplexes. The pEGFPLuc expression was finally assessed 48 h post-transfection by monitoring the fluorescent and luminescent properties of EGFP and Luc, respectively.

The gene transfection efficiency of PEI-FI-(PEG-FA) and its respective Au PENPs as analyzed by luciferase activity and EGFP expression using fluorescence microscopy are illustrated in Figure 26 and Figure 27, respectively. Taken as a whole, the same trend in cell-targeting capabilities was detected. For each vector/pDNA polyplexes, the degree of internalization into the A2780 cells was poor with or without FA-receptor blocking as can be seen by the low expression of Luc (Figure 26) and EGFP (Figure 27). Clearly, the cell-targeting capability of each FA-containing vector was not as expected. This is likely to be a result of the molar ratio of FA to PEI in the system being low.

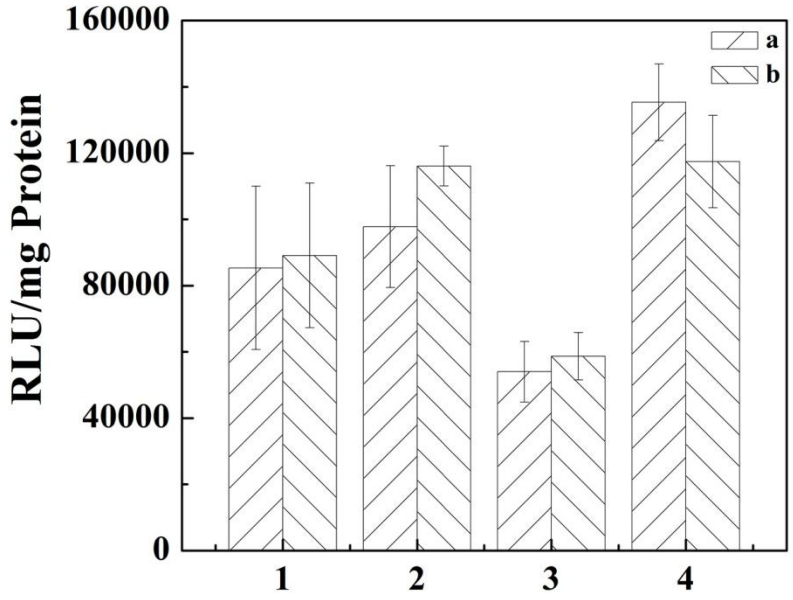

Figure 26 *In vitro* Luc gene expression in A2780 human ovarian carcinoma cells 48 h post-transfection. Cells were pre-incubated with FA 1 h prior to treatment with the polyplexes that were prepared by mixing pDNA with PEI-FI-(PEG-FA) (1), $(Au^0)_{10}$-PEI-FI-(PEG-FA) (2), $(Au^0)_{25}$-PEI-FI-(PEG-FA) (3) and $(Au^0)_{50}$-PEI-FI-(PEG-FA) (4). The cells were pre-treated without (a) and with (b) FA, respectively. All results were expressed as the mean ± SD, n =3.

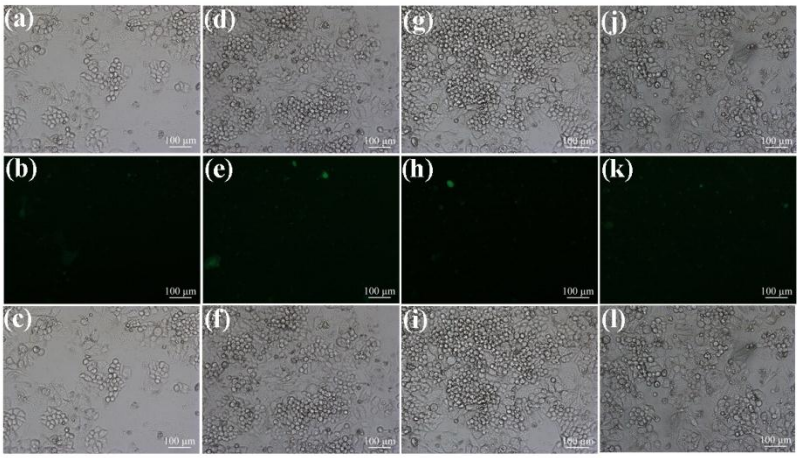

Figure 27 EGFP expression in A2780 human ovarian carcinoma cells 48 h post-transfection. Cells were pre-incubated with FA 1 h prior to treatment with the polyplexes that were prepared by mixing pDNA with PEI-FI-(PEG-FA) (a-c), $(Au^0)_{10}$-PEI-FI-(PEG-FA) (d-f), $(Au^0)_{25}$-PEI-FI-(PEG-FA) (g-i) and $(Au^0)_{50}$-PEI-FI-(PEG-FA) (j-l). Bright field images (first row), fluorescence microscopy images (second row) and the corresponding merged micrographs (third row) are shown.

Thus, it is possible that during the transfection process adsorptive endocytosis induced by the positively charged PEI is more prominent than receptor-mediated endocytosis induced by the FA moiety.

3.4 Gene silencing

3.4.1 Agarose gel electrophoresis retardation assay

Based on the gene delivery study above, for the PEI-FI-(PEG-FA) based Au PENPs, higher transfection efficiency occurred at Au atom:PEI ratio of 50:1, while higher transfection efficiency occurred at Au atom:PEI ratio of both 50:1 and 25:1 for the PEI-FI-*m*PEG based Au PENPs. Moreover, the cell viability at Au atom:PEI ratio of 50:1 was noticeably higher than that at Au atom:PEI ratio of 25:1 for the PEI-FI-(PEG-FA) based Au PENPs and the PEI-FI-*m*PEG based Au PENPs. So Au PENPs at Au atom:PEI ratio of 50:1 were selected for further study.

For cell entry to occur, compaction of siRNA by the vector system of interest is also necessary. In this experiment, the agarose gel retardation assay was used to evaluate the ability of the different vector systems that were synthesized to compact

siRNA. The principal here lies in the fact that negatively charged siRNA will migrate across the agarose gel. Upon complexation with a cationic vector via electrostatic interactions, retardation of the siRNA/vector complexes in the gel will be observed indicating the neutralization of the siRNA.

As shown in all the assays in Figure 28, a distinct band was evident at a N:P ratio of 0 indicating the migration of the negatively charged siRNA across the gel. With an increase in N:P ratio, differences in the migration of the siRNA was detected. This observation, which was evidenced in the gels by the siRNA band becoming less brilliant and eventually disappearing, was detected for all the complexes that were prepared using the vectors under investigation. For the complexes prepared using

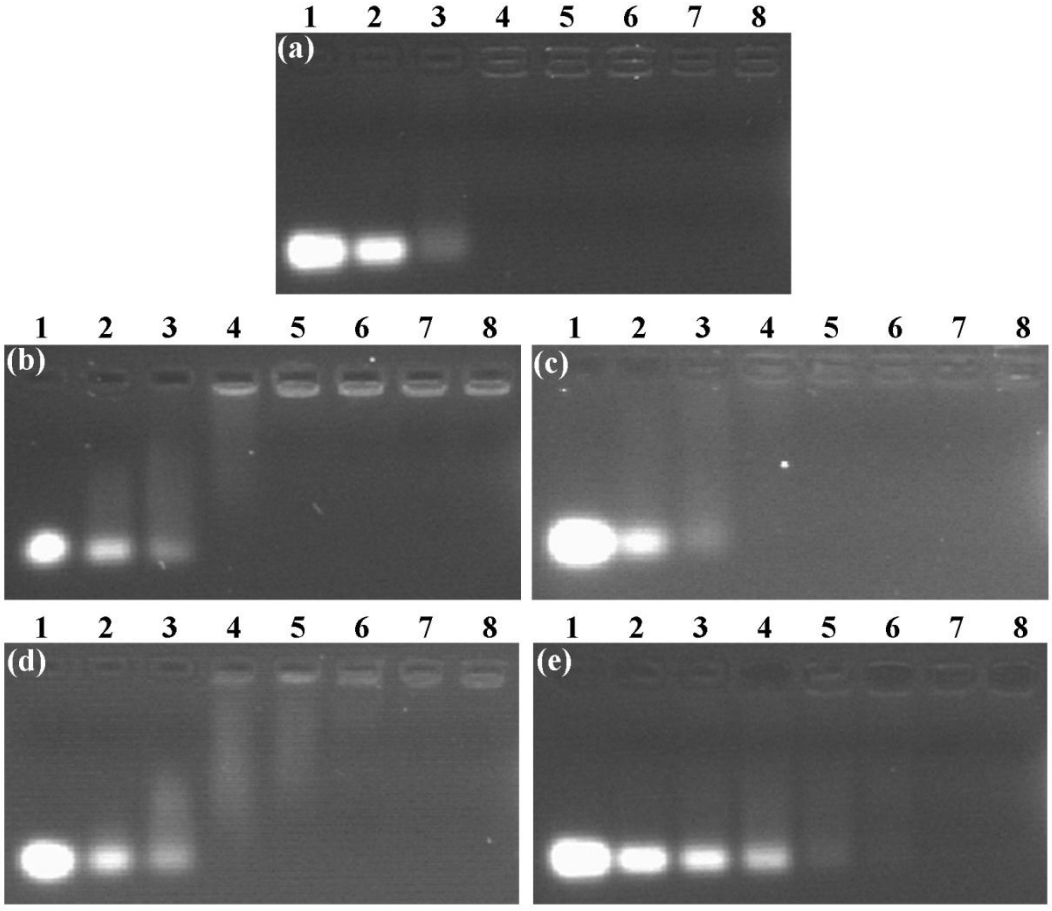

Figure 28 Gel retardation assay of siRNA complexed with PEI (a), PEI-FI-*m*PEG (b), $(Au^0)_{50}$-PEI-FI-*m*PEG (c), PEI-FI-(PEG-FA) (d), $(Au^0)_{50}$-PEI-FI-(PEG-FA) (e). For each agarose gel, N:P ratios of 0 (lane 1), 2.5 (lane 2), 5 (lane 3), 10 (lane 4), 15 (lane 5), 20 (lane 6), 25 (lane 7) and 30 (lane 8) were prepared.

PEI-FI-*m*PEG and $(Au^0)_{50}$-PEI-FI-*m*PEG, the binding and charge neutralization of siRNA occurred at a N:P ratio of 15, while the N:P ratio of 25 were selected for the complexes prepared using PEI-FI-(PEG-FA) and $(Au^0)_{50}$-PEI-FI-(PEG-FA). Compared to the compaction ability of the synthezied vectors, that of PEI were relatively higher and occurred at a N:P ratio of 10. Thus N:P ratios of 20 were selected for further study.

3.4.2 Hydrodynamic size and zeta potential measurements

The hydrodynamic size and zeta potential of siRNA-carrying vectors are also considered to be critical factors that will influence gene silencing. To this end, the DLS and zeta potential properties of such complexes can be measured in order to acquire insights into their size and zeta potential.

The hydrodynamic size of the complexes formed between siRNA with either PEI, PEI-FI-*m*PEG, $(Au^0)_{50}$-PEI-FI-*m*PEG, PEI-FI-(PEG-FA) or $(Au^0)_{50}$-PEI-FI-(PEG-FA) using the selected N:P ratios are indicated in Figure 29 (also see ANNEX I, Table 2). When compared with siRNA/PEI, the complexes formed between siRNA with PEI-FI-*m*PEG, $(Au^0)_{50}$-PEI-FI-*m*PEG and PEI-FI-(PEG-FA) were larger, while that of siRNA complexed with $(Au^0)_{50}$-PEI-FI-(PEG-FA) was smaller, which is presumably due to the influence of the FA structure or property and the entrapment of Au NPs. These complexes were in the nano-scale, which indicated that there was no aggregate in solution. The hydrodynamic radius of each sample was similar with that of siRNA/PEI complexes, so they might be uptaken by cells.

In terms of their zeta potential properties, the complexes formed between each vector under investigation with siRNA were observed to have an overall positive net charge around 23 mV (see Figure 30 and Table 2 in ANNEX I). As a result of this positive charge, each siRNA/vector complex is likely to establish electrostatic interactions with the negatively charged cell membrane, and cross it as well as subsequently introduce the negatively charged siRNA into the cell.

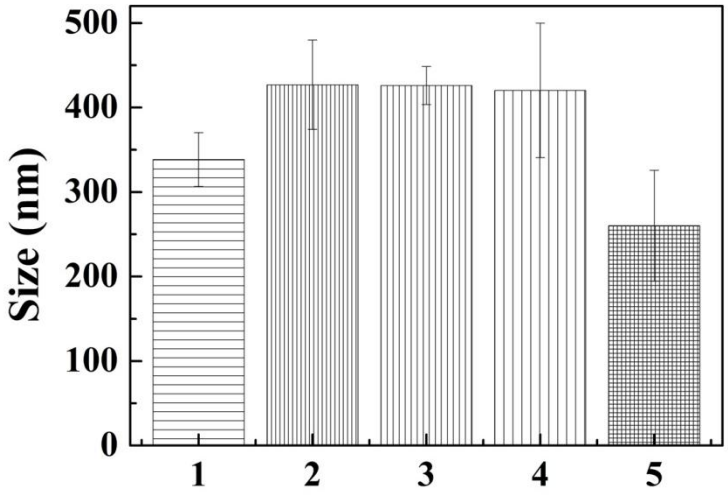

Figure 29 Hydrodynamic size of the complexes prepared by complexing siRNA with PEI (1), PEI-FI-*m*PEG (2), $(Au^0)_{50}$-PEI-FI-*m*PEG (3), PEI-FI-(PEG-FA) (4) and $(Au^0)_{50}$-PEI-FI-(PEG-FA) (5). All results were expressed as the mean ± SD, n = 3.

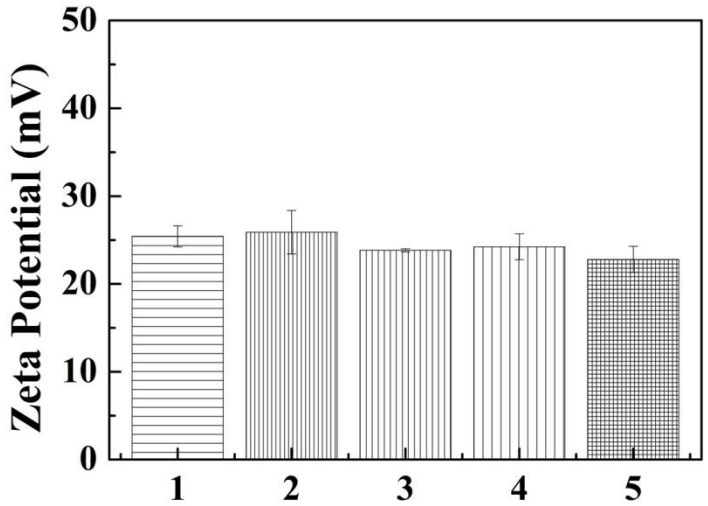

Figure 30 Zeta potential of the complexes prepared by complexing siRNA with PEI (1), PEI-FI-*m*PEG (2), $(Au^0)_{50}$-PEI-FI-*m*PEG (3), PEI-FI-(PEG-FA) (4) and $(Au^0)_{50}$-PEI-FI-(PEG-FA) (5). All results were expressed as the mean ± SD, n = 3.

3.4.3 Western blotting

Bcl-2, an endogenous regulator of apoptosis, was the first member of the bcl-2 family to be identified to play a role in inhibiting cell death under different stressful conditions.[162] The siRNA against bcl-2 mRNA can effectively induce apoptosis of lymphoma and leukemia cells through the mitochondria-mediated apoptosis pathway.[163-164] Furthermore, the expression of the bcl-2 protein has been observed in most of human cancer cell lines.[163] Therefore, the transfection of siRNA against bcl-2 may provide an efficacious approach to treat human cancer cells that express bcl-2.

Although gene silencing via RNAi technologies are considered as an important tool for therapeutic applications, the effective delivery of siRNA into cells stills presents a major challenge of gene silencing. In recent years, PEI-based materials have attracted considerable attention, owing to the ability of PEI to transport cargo molecules across the cell membrane and to promote endosomal escape. As such, this experiment focused on investigating the role of PEI-FI-*m*PEG, PEI-FI-(PEG-FA) and the respective Au PENPs in promoting gene silencing. For this, a simple and efficient method based on the western blotting techniques was used to assess the silencing of the bcl-2 siRNA through analysis of the expression of the corresponding bcl-2 protein. The tubulin protein, which was within each sample, served as an internal control.

Figure 31 shows the western blotting of bcl-2 and tubulin expression in the A2780 cells after treatment with the different complexes. For each of the vectors used, a clear difference in the expression of the bcl-2 and tubulin proteins was evident. For the primary anti-tubulin antibody that was used, the same intense bands corresponding to the 50 kDa tubulin protein were seen in the blotting for each of the prepared complexes, indicating that the tubulin protein was not silenced. For the 28 kDa bcl-2 protein on the other hand, the remarkable difference between noticeably less intense bands were evident for each complex thereby indicating that silencing of the bcl-2 gene occurred.

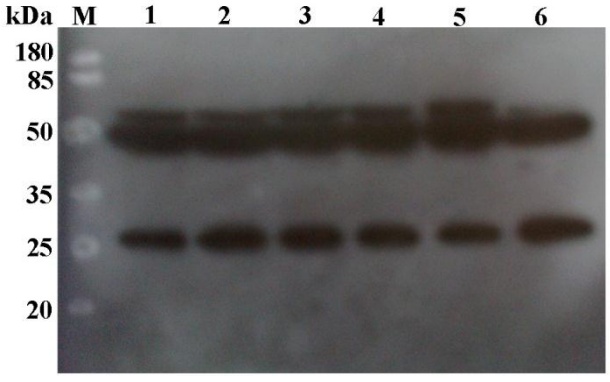

Figure 31 Western blotting evaluation of bcl-2 and tubulin expression in A2780 human ovarian carcinoma cells 48 h post-transfection. Cells were treated with complexes prepared using bcl-2 siRNA complexed with PEI (lane 1), PEI-FI-*m*PEG (lane 2), $(Au^0)_{50}$-PEI-FI-*m*PEG (lane 3), PEI-FI-(PEG-FA) (lane 4), $(Au^0)_{50}$-PEI-FI-(PEG-FA) (lane 5) and were not treated (lane 6). Lane M represented the marker. Tubulin served as an internal control for all the samples.

The data acquired is shown in the bar chart in Figure 32. Relative to PEI, clear differences in the gene silencing efficiency of the vectors was detected. The conjugation of PEG onto the PEI backbone decreased the gene silencing efficiency of the vectors (p<0.01), while the entrapment of Au NPs in the conjugates contributed to an increase in the gene silencing efficiency (p<0.01). It is likely that the entrapment of Au NPs in the PEI-FI-*m*PEG and PEI-FI-(PEG-FA) conjugates results in an increase in the accessible surface with which the siRNA can interact. Moreover, as siRNA is smaller than pDNA, siRNA can enter the remaining internal room within the Au PENPs, thereby interacting more readily with the vectors. In brief, the entrapment of Au NPs within the vector systems of interest seems to be a good idea for the gene silencing.

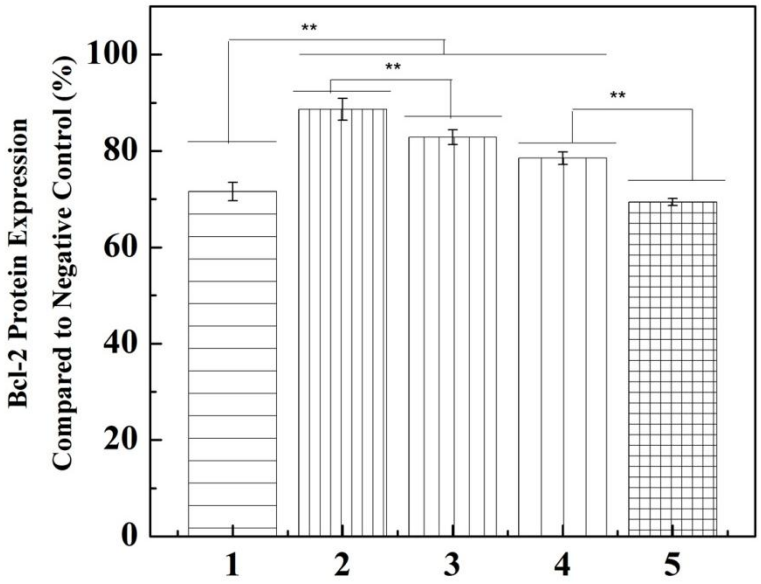

Figure 32 Western blotting analysis of gene silencing efficiency in A2780 human ovarian carcinoma cells 48 h post-transfection. Cells were treated with complexes prepared using bcl-2 siRNA complexed with PEI (1), PEI-FI-*m*PEG (2), $(Au^0)_{50}$-PEI-FI-*m*PEG (3), PEI-FI-(PEG-FA) (4) and $(Au^0)_{50}$-PEI-FI-(PEG-FA) (5).

CHAPTER 4 – GENERAL CONCLUSION

CHAPTER 4 – GENERAL CONCLUSION

In this study, a novel non-viral nucleic acid vector system was developed for enhanced and targeted nucleic acid delivery applications. In summary, PEI-FI-*m*PEG and PEI-FI-(PEG-FA) conjugates were successfully synthesized and subsequently used as templates to entrap Au NPs. The formed conjugates as well as their respective Au PENPs, were stable and were thus evaluated as vectors for the delivery of different nucleic acid types into A2780 human ovarian carcinoma cells. In the gene delivery studies, the PEI-FI-*m*PEG conjugate displayed relatively high transfection efficiency compared to PEI while the transfection efficiency of all the Au PENPs was lower. It is likely that the number of free amines and the interior room within the conjugates was decreased after Au NP entrapment. Moreover, the obvious rule of FA blocking was not shown during the transfection process, probably because the effect of electrostatic interactions was more prominent than the targeting effect. Finally, in the gene silencing studies, the results indicated that the synthesized Au PENPs with the PEGylated FA modification were good non-viral vectors for gene silencing applications in cancer cells. Overall, the results of this study provided valuable knowledge for the design of non-viral nucleic acid vectors.

REFERENCES

1. Miyata, K.; Nishiyama, N.; Kataoka, K. Rational Design of Smart Supramolecular Assemblies for Gene Delivery: Chemical Challenges in the Creation of Artificial Viruses. *Chem. Soc. Rev.* **2012,** *41*, 2562-2574.
2. Nayerossadat, N.; Maedeh, T.; Ali, P. A. Viral and Nonviral Delivery Systems for Gene Delivery. *Adv. Biomed. Res.* **2012,** *1*, 27.
3. Meacham, J. M.; Durvasula, K.; Degertekin, F. L.; Fedorov, A. G. Physical Methods for Intracellular Delivery: Practical Aspects from Laboratory Use to Industrial-Scale Processing. *J. Lab. Autom.* **2014,** *19*, 1-18.
4. Klein, T. M.; Arentzen, R.; Lewis, P. A.; Fitzpatrick-McElligott, S. Transformation of Microbes, Plants and Animals by Particle Bombardment. *Biotechnology* **1992,** *10*, 286-291.
5. Cheng, L.; Ziegelhoffer, P. R.; Yang, N. S. In Vivo Promoter Activity and Transgene Expression in Mammalian Somatic Tissues Evaluated by Using Particle Bombardment. *Proc. Natl. Acad. Sci. U. S. A.* **1993,** *90*, 4455-4459.
6. Heller, L. C.; Ugen, K.; Heller, R. Electroporation for Targeted Gene Transfer. *Expert Opin Drug Deliv.* **2005,** *2*, 255-268.
7. Plank, C.; Schillinger, U.; Scherer, F.; Bergemann, C.; Remy, J. S.; Krotz, F.; Anton, M.; Lausier, J.; Rosenecker, J. The Magnetofection Method: using Magnetic Force to Enhance Gene Delivery. *Biol. Chem.* **2003,** *384*, 737-747.
8. Scherer, F.; Anton, M.; Schillinger, U.; Henke, J.; Bergemann, C.; Kruger, A.; Gansbacher, B.; Plank, C. Magnetofection: Enhancing and Targeting Gene Delivery by Magnetic Force in Vitro and in Vivo. *Gene Ther.* **2002,** *9*, 102-109.
9. Plank, C.; Anton, M.; Rudolph, C.; Rosenecker, J.; Krotz, F. Enhancing and Targeting Nucleic Acid Delivery by Magnetic Force. *Expert Opin. Biol. Ther.* **2003,** *3*, 745-758.
10. Dobson, J. Gene Therapy Progress and Prospects: Magnetic Nanoparticle-Based Gene Delivery. *Gene Ther.* **2006,** *13*, 283-287.
11. Liang, H. D.; Lu, Q. L.; Xue, S. A.; Halliwell, M.; Kodama, T.; Cosgrove, D. O.; Stauss, H. J.; Partridge, T. A.; Blomley, M. J. Optimisation of Ultrasound-Mediated Gene Transfer (Sonoporation) in Skeletal Muscle Cells. *Ultrasound Med Biol.* **2004,** *30*, 1523-1529.
12. Huber, P. E.; Jenne, J.; Debus, J.; Wannenmacher, M. F.; Pfisterer, P. A Comparison of Shock Wave and Sinusoidal-Focused Ultrasound-Induced Localized Transfection of HeLa Cells. *Ultrasound Med Biol.* **1999,** *25*, 1451-1457.
13. Tsen, S. W.; Wu, C. Y.; Meneshian, A.; Pai, S. I.; Hung, C. F.; Wu, T. C. Femtosecond Laser Treatment Enhances DNA Transfection Efficiency in Vivo. *J Biomed Sci.* **2009,** *16*, 36.
14. Zeira, E.; Manevitch, A.; Khatchatouriants, A.; Pappo, O.; Hyam, E.; Darash-Yahana, M.; Tavor, E.; Honigman, A.; Lewis, A.; Galun, E. Femtosecond Infrared Laser-an Efficient and Safe in Vivo Gene Delivery System for Prolonged Expression. *Mol Ther.* **2003,** *8*, 342-350.
15. Kay, M. A.; Glorioso, J. C.; Naldini, L. Viral Vectors for Gene Therapy: the Art of Turning Infectious Agents into Vehicles of Therapeutics. *Nat Med.* **2001,** *7*, 33-40.
16. Barquinero, J.; Eixarch, H.; Perez-Melgosa, M. Retroviral Vectors: New Applications for an Old Tool. *Gene Ther.* **2004,** *11 Suppl 1*, S3-9.

17. Daniel, R.; Smith, J. A. Integration Site Selection by Retroviral Vectors: Molecular Mechanism and Clinical Consequences. *Hum. Gene Ther.* **2008,** *19*, 557-568.
18. St George, J. A. Gene Therapy Progress and Prospects: Adenoviral Vectors. *Gene Ther.* **2003,** *10*, 1135-1141.
19. Thomas, C. E.; Ehrhardt, A.; Kay, M. A. Progress and Problems with the Use of Viral Vectors for Gene Therapy. *Nat. Rev. Genet.* **2003,** *4*, 346-358.
20. Fire, A.; Xu, S.; Montgomery, M. K.; Kostas, S. A.; Driver, S. E.; Mello, C. C. Potent and Specific Genetic Interference by Double-Stranded RNA in Caenorhabditis Elegans. *Nature* **1998,** *391*, 806-811.
21. Bernstein, E.; Denli, A. M.; Hannon, G. J. The Rest is Silence. *Rna* **2001,** *7*, 1509-1521.
22. Scholz, C.; Wagner, E. Therapeutic Plasmid DNA Versus siRNA Delivery: Common and Different Tasks for Synthetic Carriers. *J Control Release* **2012,** *161*, 554-565.
23. Castanotto, D.; Rossi, J. J. The Promises and Pitfalls of RNA-Interference-Based Therapeutics. *Nature* **2009,** *457*, 426-433.
24. Bernstein, E.; Caudy, A. A.; Hammond, S. M.; Hannon, G. J. Role for a Bidentate Ribonuclease in the Initiation Step of RNA Interference. *Nature* **2001,** *409*, 363-366.
25. Hammond, S. M.; Bernstein, E.; Beach, D.; Hannon, G. J. An RNA-Directed Nuclease Mediates Post-Transcriptional Gene Silencing in Drosophila Cells. *Nature* **2000,** *404*, 293-296.
26. Wu, J.; Huang, W.; He, Z. Dendrimers as Carriers for siRNA Delivery and Gene Silencing: A Review. *Sci. World J.* **2013,** *2013*, 16.
27. Pack, D. W.; Hoffman, A. S.; Pun, S.; Stayton, P. S. Design and Development of Polymers for Gene Delivery. *Nat. Rev. Drug Discov* **2005,** *4*, 581-593.
28. Zhang, Y.; Satterlee, A.; Huang, L. In Vivo Gene Delivery by Nonviral Vectors: Overcoming Hurdles? *Mol. Ther.* **2012,** *20*, 1298-1304.
29. Boussif, O.; Lezoualc'h, F.; Zanta, M. A.; Mergny, M. D.; Scherman, D.; Demeneix, B.; Behr, J. P. A Versatile Vector for Gene and Oligonucleotide Transfer into Cells in Culture and In Vivo: Polyethylenimine. *Proc. Natl. Acad. Sci. U. S. A.* **1995,** *92*, 7297-7301.
30. Suh, J.; Wirtz, D.; Hanes, J. Efficient Active Transport of Gene Nanocarriers to the Cell Nucleus. *Proc. Natl. Acad. Sci. U. S. A.* **2003,** *100*, 3878-3882.
31. Gorlich, D.; Kutay, U. Transport between the Cell Nucleus and the Cytoplasm. *Annu. Rev. Cell Dev. Biol.* **1999,** *15*, 607-660.
32. Ryan, K. J.; Wente, S. R. The Nuclear Pore Complex: a Protein Machine Bridging the Nucleus and Cytoplasm. *Curr. Opin. Cell Biol.* **2000,** *12*, 361-371.
33. Aliabadi, H. M.; Landry, B.; Sun, C.; Tang, T.; Uludağ, H. Supramolecular Assemblies in Functional siRNA Delivery: Where Do We Stand? *Biomaterials* **2012,** *33*, 2546-2569.
34. Kobayashi, H.; Watanabe, R.; Choyke, P. L. Improving Conventional Enhanced Permeability and Retention (EPR) Effects; What Is the Appropriate Target? *Theranostics* **2014,** *4*, 81-89.
35. Xiao, T.; Hou, W.; Cao, X.; Wen, S.; Shen, M.; Shi, X. Dendrimer-Entrapped Gold Nanoparticles Modified with Folic Acid for Targeted Gene Delivery Applications. *Biomater. Sci.* **2013,** *1*, 1172-1180.
36. Kim, H.-K.; Wei, H.; Kulkarni, A.; Pogranichniy, R. M.; Thompson, D. H. Effective Targeted Gene Delivery to Dendritic Cells via Synergetic Interaction of Mannosylated Lipid with DOPE and BCAT. *Biomacromolecules* **2012,** *13*, 636-644.

37. Ong, Z. Y.; Yang, C.; Gao, S. J.; Ke, X. Y.; Hedrick, J. L.; Yan Yang, Y. Galactose-Functionalized Cationic Polycarbonate Diblock Copolymer for Targeted Gene Delivery to Hepatocytes. *Macromol. Rapid Commun.* **2013,** *34*, 1714-1720.
38. Schiffelers, R. M.; Ansari, A.; Xu, J.; Zhou, Q.; Tang, Q.; Storm, G.; Molema, G.; Lu, P. Y.; Scaria, P. V.; Woodle, M. C. Cancer siRNA Therapy by Tumor Selective Delivery with Ligand-Targeted Sterically Stabilized Nanoparticle. *Nucleic Acids Res.* **2004,** *32*, e149.
39. Lee, K. M.; Kim, I. S.; Lee, Y. B.; Shin, S. C.; Lee, K. C.; Oh, I. J. Evaluation of Transferrin-Polyethylenimine Conjugate for Targeted Gene Delivery. *Arch Pharm Res.* **2005,** *28*, 722-729.
40. Shiota, M.; Ikeda, Y.; Kaul, Z.; Itadani, J.; Kaul, S. C.; Wadhwa, R. Internalizing Antibody-Based Targeted Gene Delivery for Human Cancer Cells. *Hum. Gene Ther.* **2007,** *18*, 1153-1160.
41. Chen, S.; Zhao, X.; Chen, J.; Chen, J.; Kuznetsova, L.; Wong, S. S.; Ojima, I. Mechanism-Based Tumor-Targeting Drug Delivery System. Validation of Efficient Vitamin Receptor-Mediated Endocytosis and Drug Release. *Bioconjugate Chem.* **2010,** *21*, 979-987.
42. Farokhzad, O. C.; Cheng, J.; Teply, B. A.; Sherifi, I.; Jon, S.; Kantoff, P. W.; Richie, J. P.; Langer, R. Targeted Nanoparticle-Aptamer Bioconjugates for Cancer Chemotherapy in Vivo. *Proc. Natl. Acad. Sci. U. S. A.* **2006,** *103*, 6315-6320.
43. Su, C. H.; Wu, Y. J.; Wang, H. H.; Yeh, H. I. Nonviral Gene Therapy Targeting Cardiovascular System. *Am J Physiol Heart Circ Physiol* **2012,** *303*, H629-638.
44. Lu, Q. L.; Bou-Gharios, G.; Partridge, T. A. Non-Viral Gene Delivery in Skeletal Muscle: a Protein Factory. *Gene Ther.* **2003,** *10*, 131-142.
45. Davis, P.; Ziady, A. Non-Viral Methods of Gene Transfer to Airway Epithelium. *Gene Ther. Regul.* **2003,** *2*, 77-90.
46. Park, T. G.; Jeong, J. H.; Kim, S. W. Current Status of Polymeric Gene Delivery Systems. *Adv. Drug Delivery Rev.* **2006,** *58*, 467-486.
47. Elsabahy, M.; Nazarali, A.; Foldvari, M. Non-Viral Nucleic Acid Delivery: Key Challenges and Future Directions. *Curr. Drug Delivery* **2011,** *8*, 235-244.
48. Zhou, R.; Geiger, R. C.; Dean, D. A. Intracellular Trafficking of Nucleic Acids. *Expert Opin Drug Deliv.* **2004,** *1*, 127-140.
49. Brunner, S.; Sauer, T.; Carotta, S.; Cotten, M.; Saltik, M.; Wagner, E. Cell Cycle Dependence of Gene Transfer by Lipoplex, Polyplex and Recombinant Adenovirus. *Gene Ther.* **2000,** *7*, 401-407.
50. Pollard, H.; Remy, J. S.; Loussouarn, G.; Demolombe, S.; Behr, J. P.; Escande, D. Polyethylenimine but not Cationic Lipids Promotes Transgene Delivery to the Nucleus in Mammalian Cells. *J. Biol. Chem.* **1998,** *273*, 7507-7511.
51. Godbey, W. T.; Wu, K. K.; Mikos, A. G. Tracking the Intracellular Path of Poly(ethylenimine)/DNA Complexes for Gene Delivery. *Proc. Natl. Acad. Sci. U. S. A.* **1999,** *96*, 5177-5181.
52. Brunner, S.; Furtbauer, E.; Sauer, T.; Kursa, M.; Wagner, E. Overcoming the Nuclear Barrier: Cell Cycle Independent Nonviral Gene Transfer with Linear Polyethylenimine or Electroporation. *Mol Ther.* **2002,** *5*, 80-86.
53. Oh, Y. K.; Suh, D.; Kim, J. M.; Choi, H. G.; Shin, K.; Ko, J. J. Polyethylenimine-Mediated Cellular Uptake, Nucleus Trafficking and Expression of Cytokine Plasmid DNA. *Gene Ther.*

2002, *9*, 1627-1632.

54. Remy-Kristensen, A.; Clamme, J. P.; Vuilleumier, C.; Kuhry, J. G.; Mely, Y. Role of Endocytosis in the Transfection of L929 Fibroblasts by Polyethylenimine/DNA Complexes. *Biochim. Biophys. Acta* **2001,** *1514*, 21-32.
55. Mannisto, M.; Ronkko, S.; Matto, M.; Honkakoski, P.; Hyttinen, M.; Pelkonen, J.; Urtti, A. The Role of Cell Cycle on Polyplex-Mediated Gene Transfer into a Retinal Pigment Epithelial Cell Line. *J. Gene Med.* **2005,** *7*, 466-476.
56. Chu, M.; Dong, C.; Zhu, H.; Cai, X.; Dong, H.; Ren, T.; Su, J.; Li, Y. Biocompatible Polyethylenimine-Graft-Dextran Catiomer for Highly Efficient Gene Delivery Assisted by a Nuclear Targeting Ligand. *Polym. Chem.* **2013,** *4*, 2528-2539.
57. Shim, M. S.; Kwon, Y. J. Controlled Cytoplasmic and Nuclear Localization of Plasmid DNA and siRNA by Differentially Tailored Polyethylenimine. *J. Controlled Release* **2009,** *133*, 206-213.
58. Grosse, S.; Thevenot, G.; Monsigny, M.; Fajac, I. Which Mechanism for Nuclear Import of Plasmid DNA Complexed with Polyethylenimine Derivatives? *J. Gene Med.* **2006,** *8*, 845-851.
59. Kang, B.; Mackey, M. A.; El-Sayed, M. A. Nuclear Targeting of Gold Nanoparticles in Cancer Cells Induces DNA Damage, Causing Cytokinesis Arrest and Apoptosis. *J. Am. Chem. Soc.* **2010,** *132*, 1517-1519.
60. Dam, D. H. M.; Lee, J. H.; Sisco, P. N.; Co, D. T.; Zhang, M.; Wasielewski, M. R.; Odom, T. W. Direct Observation of Nanoparticle–Cancer Cell Nucleus Interactions. *ACS Nano* **2012,** *6*, 3318-3326.
61. Huo, S.; Jin, S.; Ma, X.; Xue, X.; Yang, K.; Kumar, A.; Wang, P. C.; Zhang, J.; Hu, Z.; Liang, X.-J. Ultrasmall Gold Nanoparticles as Carriers for Nucleus-Based Gene Therapy Due to Size-Dependent Nuclear Entry. *ACS Nano* **2014,** *8*, 5852-5862.
62. Choi, S.; Jung, S.; Ryu, P.; Joo, S.; Lee, S. Branched Polyethyleneimine Coating Gold Nanoparticle-Mediated Gene Delivery Targeting Nuclear Protein in A_{549} Cells. *FASEB J.* **2012,** *26*, 580.510.
63. Liu, X.; Rocchi, P.; Peng, L. Dendrimers as Non-Viral Vectors for siRNA Delivery. *New J. Chem.* **2012,** *36*, 256-263.
64. Felgner, P. L.; Gadek, T. R.; Holm, M.; Roman, R.; Chan, H. W.; Wenz, M.; Northrop, J. P.; Ringold, G. M.; Danielsen, M. Lipofection: a Highly Efficient, Lipid-Mediated DNA-Transfection Procedure. *Proc. Natl. Acad. Sci. U. S. A.* **1987,** *84*, 7413-7417.
65. Merdan, T.; Kopeček, J.; Kissel, T. Prospects for Cationic Polymers in Gene and Oligonucleotide Therapy Against Cancer. *Adv. Drug Delivery Rev.* **2002,** *54*, 715-758.
66. Lin, G.; Zhang, H.; Huang, L. Smart Polymeric Nanoparticles for Cancer Gene Delivery. *Mol. Pharmaceutics* **2015,** *12*, 314-321.
67. Sunshine, J. C.; Bishop, C. J.; Green, J. J. Advances in Polymeric and Inorganic Vectors for Nonviral Nucleic Acid Delivery. *Ther. Delivery* **2011,** *2*, 493-521.
68. Patnaik, S.; Aggarwal, A.; Nimesh, S.; Goel, A.; Ganguli, M.; Saini, N.; Singh, Y.; Gupta, K. C. PEI-Alginate Nanocomposites as Efficient in Vitro Gene Transfection Agents. *J. Controlled Release* **2006,** *114*, 398-409.
69. Garnett, M. C. Gene-Delivery Systems using Cationic Polymers. *Crit. Rev. Ther. Drug Carrier Syst.* **1999,** *16*, 147-207.

70. Behr, J.-P. The Proton Sponge: a Trick to Enter Cells the Viruses Did Not Exploit. *CHIMIA International Journal for Chemistry* **1997,** *51*, 34-36.
71. Nel, A. E.; Madler, L.; Velegol, D.; Xia, T.; Hoek, E. M. V.; Somasundaran, P.; Klaessig, F.; Castranova, V.; Thompson, M. Understanding Biophysicochemical Interactions at the Nano-Bio Interface. *Nat. Mater.* **2009,** *8*, 543-557.
72. Benjaminsen, R. V.; Mattebjerg, M. A.; Henriksen, J. R.; Moghimi, S. M.; Andresen, T. L. The Possible "Proton Sponge " Effect of Polyethylenimine (PEI) Does Not Include Change in Lysosomal pH. *Mol. Ther.* **2013,** *21*, 149-157.
73. http://en.wikipedia.org/wiki/Polyethylenimine
74. Godbey, W. T.; Wu, K. K.; Mikos, A. G. Poly(ethylenimine)-Mediated Gene Delivery Affects Endothelial Cell Function and Viability. *Biomaterials* **2001,** *22*, 471-480.
75. Moghimi, S. M.; Symonds, P.; Murray, J. C.; Hunter, A. C.; Debska, G.; Szewczyk, A. A Two-Stage Poly(ethylenimine)-Mediated Cytotoxicity: Implications for Gene Transfer/Therapy. *Mol Ther.* **2005,** *11*, 990-995.
76. Boeckle, S.; von Gersdorff, K.; van der Piepen, S.; Culmsee, C.; Wagner, E.; Ogris, M. Purification of Polyethylenimine Polyplexes Highlights the Role of Free Polycations in Gene Transfer. *J. Gene Med.* **2004,** *6*, 1102-1111.
77. Thomas, M.; Klibanov, A. M. Enhancing Polyethylenimine's Delivery of Plasmid DNA into Mammalian Cells. *Proc. Natl. Acad. Sci. U. S. A.* **2002,** *99*, 14640-14645.
78. Ahn, C.-H.; Chae, S. Y.; Bae, Y. H.; Kim, S. W. Biodegradable Poly(ethylenimine) for Plasmid DNA Delivery. *J. Controlled Release* **2002,** *80*, 273-282.
79. Mishra, S.; Webster, P.; Davis, M. E. PEGylation Significantly Affects Cellular Uptake and Intracellular Trafficking of Non-Viral Gene Delivery Particles. *Eur. J. Cell Biol.* **2004,** *83*, 97-111.
80. Mu, Q.; Hu, T.; Yu, J. Molecular Insight into the Steric Shielding Effect of PEG on the Conjugated Staphylokinase: Biochemical Characterization and Molecular Dynamics Simulation. *PLoS One* **2013,** *8*, e68559.
81. Nouri, A.; Castro, R.; Kairys, V.; Santos, J. L.; Rodrigues, J.; Li, Y.; Tomas, H. Insight into the Role of N,N-Dimethylaminoethyl Methacrylate (DMAEMA) Conjugation onto Poly(ethylenimine): Cell Viability and Gene Transfection Studies. *J Mater Sci Mater Med* **2012,** *23*, 2967-2980.
82. Jiang, D.; Salem, A. K. Optimized Dextran-Polyethylenimine Conjugates are Efficient Non-Viral Vectors with Reduced Cytotoxicity When Used in Serum Containing Environments. *Int. J. Pharm.* **2012,** *427*, 71-79.
83. Song, H.; Wang, G.; He, B.; Li, L.; Li, C.; Lai, Y.; Xu, X.; Gu, Z. Cationic Lipid-Coated PEI/DNA Polyplexes with Improved Efficiency and Reduced Cytotoxicity for Gene Delivery into Mesenchymal Stem Cells. *Int. J. Nanomed.* **2012,** *7*, 4637-4648.
84. Wang, Y.; Zheng, M.; Meng, F.; Zhang, J.; Peng, R.; Zhong, Z. Branched Polyethylenimine Derivatives with Reductively Cleavable Periphery for Safe and Efficient In Vitro Gene Transfer. *Biomacromolecules* **2011,** *12*, 1032-1040.
85. Tian, H.; Li, F.; Chen, J.; Huang, Y.; Chen, X. N-Isopropylacrylamide-Modified Polyethylenimines as Effective Gene Carriers. *Macromol. Biosci.* **2012,** *12*, 1680-1688.
86. Yeh, Y.-C.; Creran, B.; Rotello, V. M. Gold Nanoparticles: Preparation, Properties, and Applications in Bionanotechnology. *Nanoscale* **2012,** *4*, 1871-1880.

87. Kumar, A.; Boruah, B. M.; Liang, X.-J. Gold Nanoparticles: Promising Nanomaterials for the Diagnosis of Cancer and HIV/AIDS. *J. Nanomater.* **2011,** *2011*, 22.

88. Abdelhalim, M. A. K.; Mady, M. M.; Ghannam, M. M. Physical Properties of Different Gold Nanoparticles: Ultraviolet-Visible and Fluorescence Measurements. *J Nanomed Nanotechol* **2012,** *3*, 2.

89. Huang, X.; El-Sayed, M. A. Gold Nanoparticles: Optical Properties and Implementations in Cancer Diagnosis and Photothermal Therapy. *J. Adv. Res.* **2010,** *1*, 13-28.

90. Hendel, T.; Wuithschick, M.; Kettemann, F.; Birnbaum, A.; Rademann, K.; Polte, J. In Situ Determination of Colloidal Gold Concentrations with UV−Vis Spectroscopy: Limitations and Perspectives. *Anal. Chem.* **2014,** *86*, 11115-11124.

91. Jiang, X.; Housni, A.; Gody, G.; Boullanger, P.; Charreyre, M. T.; Delair, T.; Narain, R. Synthesis of Biotinylated Alpha-d-Mannoside or N-Acetyl Beta-d-Glucosaminoside Decorated Gold Nanoparticles: Study of Their Biomolecular Recognition with Con A and WGA Lectins. *Bioconjugate Chem.* **2010,** *21*, 521-530.

92. Zheng, M.; Huang, X. Nanoparticles Comprising a Mixed Monolayer for Specific Bindings with Biomolecules. *J. Am. Chem. Soc.* **2004,** *126*, 12047-12054.

93. Ghosh, P.; Yang, X.; Arvizo, R.; Zhu, Z. J.; Agasti, S. S.; Mo, Z.; Rotello, V. M. Intracellular Delivery of a Membrane-Impermeable Enzyme in Active Form using Functionalized Gold Nanoparticles. *J. Am. Chem. Soc.* **2010,** *132*, 2642-2645.

94. Samanta, B.; Yang, X. C.; Ofir, Y.; Park, M. H.; Patra, D.; Agasti, S. S.; Miranda, O. R.; Mo, Z. H.; Rotello, V. M. Catalytic Microcapsules Assembled from Enzyme-Nanoparticle Conjugates at Oil-Water Interfaces. *Angew. Chem., Int. Ed. Engl.* **2009,** *48*, 5341-5344.

95. Cardenas, M.; Barauskas, J.; Schillen, K.; Brennan, J. L.; Brust, M.; Nylander, T. Thiol-Specific and Nonspecific Interactions between DNA and Gold Nanoparticles. *Langmuir* **2006,** *22*, 3294-3299.

96. Li, X.; Guo, J.; Asong, J.; Wolfert, M. A.; Boons, G. J. Multifunctional Surface Modification of Gold-Stabilized Nanoparticles by Bioorthogonal Reactions. *J. Am. Chem. Soc.* **2011,** *133*, 11147-11153.

97. Dykman, L.; Khlebtsov, N. Gold Nanoparticles in Biomedical Applications: Recent Advances and Perspectives. *Chem. Soc. Rev.* **2012,** *41*, 2256-2282.

98. Turkevich, J.; Stevenson, P. C.; Hillier, J. A Study of the Nucleation and Growth Processes in the Synthesis of Colloidal Gold. *Discuss. Faraday Soc.* **1951,** *11*, 55-75.

99. Frens, G. Controlled Nucleation for the Regulation of the Particle Size in Monodisperse Gold Suspensions. *Nature* **1972**, 20-22.

100. Park, J.-W.; Shumaker-Parry, J. S. Structural Study of Citrate Layers on Gold Nanoparticles: Role of Intermolecular Interactions in Stabilizing Nanoparticles. *J. Am. Chem. Soc.* **2014,** *136*, 1907-1921.

101. Aslan, K.; Pérez-Luna, V. H. Surface Modification of Colloidal Gold by Chemisorption of Alkanethiols in the Presence of a Nonionic Surfactant. *Langmuir* **2002,** *18*, 6059-6065.

102. Lin, S.-Y.; Tsai, Y.-T.; Chen, C.-C.; Lin, C.-M.; Chen, C.-h. Two-Step Functionalization of Neutral and Positively Charged Thiols onto Citrate-Stabilized Au Nanoparticles. *J. Phys. Chem. B* **2004,** *108*, 2134-2139.

103. Brust, M.; Walker, M.; Bethell, D.; Schiffrin, D. J.; Whyman, R. Synthesis of Thiol-Derivatised Gold Nanoparticles in a Two-Phase Liquid-Liquid System. *J. Chem. Soc.*,

Chem. Commun. **1994**, 801-802.

104. Faraday, M. The Bakerian Lecture: Experimental Relations of Gold (and Other Metals) to Light. *Philos. Trans. R. Soc. London* **1857,** *147*, 145-181.
105. Porter, M. D.; Bright, T. B.; Allara, D. L.; Chidsey, C. E. D. Spontaneously Organized Molecular Assemblies. 4. Structural Characterization of N-Alkyl Thiol Monolayers on Gold by Optical Ellipsometry, Infrared Spectroscopy, and Electrochemistry. *J. Am. Chem. Soc.* **1987,** *109*, 3559-3568.
106. Laibinis, P. E.; Nuzzo, R. G.; Whitesides, G. M. Structure of Monolayers Formed by Coadsorption of Two N-Alkanethiols of Different Chain Lengths on Gold and Its Relation to Wetting. *J. Phys. Chem.* **1992,** *96*, 5097-5105.
107. Hostetler, M. J.; Wingate, J. E.; Zhong, C.-J.; Harris, J. E.; Vachet, R. W.; Clark, M. R.; Londono, J. D.; Green, S. J.; Stokes, J. J.; Wignall, G. D.; Glish, G. L.; Porter, M. D.; Evans, N. D.; Murray, R. W. Alkanethiolate Gold Cluster Molecules with Core Diameters from 1.5 to 5.2 nm: Core and Monolayer Properties as a Function of Core Size. *Langmuir* **1998,** *14*, 17-30.
108. Love, J. C.; Estroff, L. A.; Kriebel, J. K.; Nuzzo, R. G.; Whitesides, G. M. Self-Assembled Monolayers of Thiolates on Metals as a Form of Nanotechnology. *Chem. Rev.* **2005,** *105*, 1103-1170.
109. Rowe, M. P.; Plass, K. E.; Kim, K.; Kurdak, Ç.; Zellers, E. T.; Matzger, A. J. Single-Phase Synthesis of Functionalized Gold Nanoparticles. *Chem. Mater.* **2004,** *16*, 3513-3517.
110. Ji, X.; Song, X.; Li, J.; Bai, Y.; Yang, W.; Peng, X. Size Control of Gold Nanocrystals in Citrate Reduction: The Third Role of Citrate. *J. Am. Chem. Soc.* **2007,** *129*, 13939-13948.
111. Nikoobakht, B.; El-Sayed, M. A. Preparation and Growth Mechanism of Gold Nanorods (NRs) Using Seed-Mediated Growth Method. *Chem. Mater.* **2003,** *15*, 1957-1962.
112. Zhang, A.-Q.; Cai, L.-J.; Sui, L.; Qian, D.-J.; Chen, M. Reducing Properties of Polymers in the Synthesis of Noble Metal Nanoparticles. *Polym. Rev.* **2013,** *53*, 240-276.
113. Zhou, M.; Wang, B.; Rozynek, Z.; Xie, Z.; Fossum, J. O.; Yu, X.; Raaen, S. Minute Synthesis of Extremely Stable Gold Nanoparticles. *Nanotechnology* **2009,** *20*, 505606.
114. Washio, I.; Xiong, Y.; Yin, Y.; Xia, Y. Reduction by the End Groups of Poly(vinyl pyrrolidone): A New and Versatile Route to the Kinetically Controlled Synthesis of Ag Triangular Nanoplates. *Adv. Mater.* **2006,** *18*, 1745-1749.
115. Lim, B.; Camargo, P. H. C.; Xia, Y. Mechanistic Study of the Synthesis of Au Nanotadpoles, Nanokites, and Microplates by Reducing Aqueous $HAuCl_4$ with Poly(vinyl pyrrolidone). *Langmuir* **2008,** *24*, 10437-10442.
116. Huang, H. H.; Ni, X. P.; Loy, G. L.; Chew, C. H.; Tan, K. L.; Loh, F. C.; Deng, J. F.; Xu, G. Q. Photochemical Formation of Silver Nanoparticles in Poly(N-vinylpyrrolidone). *Langmuir* **1996,** *12*, 909-912.
117. Deng, Z.; Chen, M.; Wu, L. Novel Method to Fabricate SiO_2/Ag Composite Spheres and Their Catalytic, Surface-Enhanced Raman Scattering Properties. *J. Phys. Chem. C* **2007,** *111*, 11692-11698.
118. Ram, S.; Fecht, H. J. Modulating Up-Energy Transfer and Violet-Blue Light Emission in Gold Nanoparticles with Surface Adsorption of Poly(vinyl pyrrolidone) Molecules. *J. Phys. Chem. C* **2011,** *115*, 7817-7828.
119. Shan, Y.; Luo, T.; Peng, C.; Sheng, R.; Cao, A.; Cao, X.; Shen, M.; Guo, R.; Tomás, H.; Shi, X.

Gene Delivery using Dendrimer-Entrapped Gold Nanoparticles as Nonviral Vectors. *Biomaterials* **2012,** *33*, 3025-3035.

120. Scott, R. W.; Wilson, O. M.; Crooks, R. M. Synthesis, Characterization, and Applications of Dendrimer-Encapsulated Nanoparticles. *J. Phys. Chem. B* **2005,** *109*, 692-704.
121. Guo, R.; Wang, H.; Peng, C.; Shen, M.; Pan, M.; Cao, X.; Zhang, G.; Shi, X. X-ray Attenuation Property of Dendrimer-Entrapped Gold Nanoparticles. *J. Phys. Chem. C* **2010,** *114*, 50-56.
122. Wu, Y.; Wang, W.; Chen, Y.; Huang, K.; Shuai, X.; Chen, Q.; Li, X.; Lian, G. The Investigation of Polymer-siRNA Nanoparticle for Gene Therapy of Gastric Cancer in Vitro. *Int. J. Nanomed.* **2010,** *5*, 129-136.
123. Gröhn, F.; Bauer, B. J.; Akpalu, Y. A.; Jackson, C. L.; Amis, E. J. Dendrimer Templates for the Formation of Gold Nanoclusters. *Macromolecules* **2000,** *33*, 6042-6050.
124. Mikami, T.; Takayasu, Y.; Hirasawa, I. PEI-Assisted Preparation of Au Nanoparticles via Reductive Crystallization Process. *Chem. Eng. Res. Des.* **2010,** *88*, 1248-1251.
125. Chen, C.-C.; Kuo, P.-L. Gold Nanoparticles Prepared using Polyethylenimine Adsorbed onto Montmorillonite. *J. Colloid Interface Sci.* **2006,** *293*, 101-107.
126. Luo, Y. Size-Controlled Preparation of Polyelectrolyte-Protected Gold Nanoparticles by Natural Sunlight Radiation. *Mater. Lett.* **2007,** *61*, 2164-2166.
127. Song, W. J.; Du, J. Z.; Sun, T. M.; Zhang, P. Z.; Wang, J. Gold Nanoparticles Capped with Polyethyleneimine for Enhanced siRNA Delivery. *Small* **2010,** *6*, 239-246.
128. McCaffrey, R.; Long, H.; Jin, Y.; Sanders, A.; Park, W.; Zhang, W. Template Synthesis of Gold Nanoparticles with an Organic Molecular Cage. *J. Am. Chem. Soc.* **2014,** *136*, 1782-1785.
129. Xie, J.; Lee, S.; Chen, X. Nanoparticle-Based Theranostic Agents. *Adv. Drug Delivery Rev.* **2010,** *62*, 1064-1079.
130. Bishop, C. J.; Tzeng, S. Y.; Green, J. J. Degradable Polymer-Coated Gold Nanoparticles for Co-Delivery of DNA and siRNA. *Acta Biomater.* **2015,** *11*, 393-403.
131. Hu, C.; Peng, Q.; Chen, F.; Zhong, Z.; Zhuo, R. Low Molecular Weight Polyethylenimine Conjugated Gold Nanoparticles as Efficient Gene Vectors. *Bioconjugate Chem.* **2010,** *21*, 836-843.
132. Ding, Y.; Jiang, Z.; Saha, K.; Kim, C. S.; Kim, S. T.; Landis, R. F.; Rotello, V. M. Gold Nanoparticles for Nucleic Acid Delivery. *Mol Ther.* **2014,** *22*, 1075-1083.
133. Kobayashi, K.; Wei, J.; Iida, R.; Ijiro, K.; Niikura, K. Surface Engineering of Nanoparticles for Therapeutic Applications. *Polym. J.* **2014,** *46*, 460-468.
134. Sharma, A.; Tandon, A.; Tovey, J. C.; Gupta, R.; Robertson, J. D.; Fortune, J. A.; Klibanov, A. M.; Cowden, J. W.; Rieger, F. G.; Mohan, R. R. Polyethylenimine-Conjugated Gold Nanoparticles: Gene Transfer Potential and Low Toxicity in the Cornea. *Nanomedicine* **2011,** *7*, 505-513.
135. Thomas, M.; Klibanov, A. M. Conjugation to Gold Nanoparticles Enhances Polyethylenimine's Transfer of Plasmid DNA into Mammalian Cells. *Proc. Natl. Acad. Sci. U. S. A.* **2003,** *100*, 9138-9143.
136. Lee, Y.; Lee, S. H.; Kim, J. S.; Maruyama, A.; Chen, X.; Park, T. G. Controlled Synthesis of PEI-Coated Gold Nanoparticles using Reductive Catechol Chemistry for siRNA Delivery. *J Control Release* **2011,** *155*, 3-10.
137. Mitra, M.; Kandalam, M.; Rangasamy, J.; Shankar, B.; Maheswari, U. K.; Swaminathan, S.;

Krishnakumar, S. Novel Epithelial Cell Adhesion Molecule Antibody Conjugated Polyethyleneimine-Capped Gold Nanoparticles for Enhanced and Targeted Small Interfering RNA Delivery to Retinoblastoma Cells. *Mol. Vision* **2013,** *19*, 1029-1038.

138. Guo, S.; Huang, Y.; Jiang, Q.; Sun, Y.; Deng, L.; Liang, Z.; Du, Q.; Xing, J.; Zhao, Y.; Wang, P. C.; Dong, A.; Liang, X. J. Enhanced Gene Delivery and siRNA Silencing by Gold Nanoparticles Coated with Charge-Reversal Polyelectrolyte. *ACS Nano* **2010,** *4*, 5505-5511.
139. Li, J.; Zheng, L.; Cai, H.; Sun, W.; Shen, M.; Zhang, G.; Shi, X. Polyethyleneimine-Mediated Synthesis of Folic Acid-Targeted Iron Oxide Nanoparticles for in Vivo Tumor MR Imaging. *Biomaterials* **2013,** *34*, 8382-8392.
140. Tong, W.; Cao, X.; Wen, S.; Guo, R.; Shen, M.; Wang, J.; Shi, X. Enhancing the Specificity and Efficiency of Polymerase Chain Reaction using Polyethyleneimine-Based Derivatives and Hybrid Nanocomposites. *Int. J. Nanomed.* **2012,** *7*, 1069-1078.
141. Wen, S.; Li, K.; Cai, H.; Chen, Q.; Shen, M.; Huang, Y.; Peng, C.; Hou, W.; Zhu, M.; Zhang, G.; Shi, X. Multifunctional Dendrimer-Entrapped Gold Nanoparticles for Dual Mode CT/MR Imaging Applications. *Biomaterials* **2013,** *34*, 1570-1580.
142. Liang, W.; Mason, A. J.; Lam, J. K. W. Western Blot Evaluation of siRNA Delivery by pH Responsive Peptides. *Methods Mol Biol.* **2013,** *986*, 73-87.
143. Yin, H.; Kanasty, R. L.; Eltoukhy, A. A.; Vegas, A. J.; Dorkin, J. R.; Anderson, D. G. Non-Viral Vectors for Gene-Based Therapy. *Nat Rev Genet* **2014,** *15*, 541-555.
144. Holycross, D. R.; Chai, M. Comprehensive NMR Studies of the Structures and Properties of PEI Polymers. *Macromolecules* **2013,** *46*, 6891-6897.
145. Bi, X.; Shi, X.; Baker, J. R., Jr. Synthesis, Characterization and Stability of a Luteinizing Hormone-Releasing Hormone (LHRH)-Functionalized Poly(amidoamine) Dendrimer Conjugate. *J Biomater Sci Polym Ed* **2008,** *19*, 131-142.
146. Zhou, B.; Zheng, L.; Peng, C.; Li, D.; Li, J.; Wen, S.; Shen, M.; Zhang, G.; Shi, X. Synthesis and Characterization of PEGylated Polyethylenimine-Entrapped Gold Nanoparticles for Blood Pool and Tumor CT Imaging. *ACS Appl Mater Interfaces* **2014,** *6*, 17190-17199.
147. Zhang, D.; Vangala, K.; Jiang, D.; Zou, S.; Pechan, T. Drop Coating Deposition Raman Spectroscopy of Fluorescein Isothiocyanate Labeled Protein. *Appl. Spectrosc.* **2010,** *64*, 1078-1085.
148. Zwicke, G. L.; Mansoori, G. A.; Jeffery, C. J. Utilizing the Folate Receptor for Active Targeting of Cancer Nanotherapeutics. *Nano Rev.* **2012,** *3*, 10.3402/nano.v3403i3400.18496.
149. Pan, D.; Turner, J. L.; Wooley, K. L. Folic Acid-Conjugated Nanostructured Materials Designed for Cancer Cell Targeting. *Chem. Commun.* **2003**, 2400-2401.
150. Shakeri-Zadeh, A.; Ghasemifard, M.; Ali Mansoori, G. Structural and Optical Characterization of Folate-Conjugated Gold-Nanoparticles. *Phys. E* **2010,** *42*, 1272-1280.
151. Duran, M. C.; Willenbrock, S.; Barchanski, A.; Muller, J. M.; Maiolini, A.; Soller, J. T.; Barcikowski, S.; Nolte, I.; Feige, K.; Murua Escobar, H. Comparison of Nanoparticle-Mediated Transfection Methods for DNA Expression Plasmids: Efficiency and Cytotoxicity. *J Nanobiotechnology* **2011,** *9*, 47.
152. Shi, X.; Wang, S. H.; Van Antwerp, M. E.; Chen, X.; Baker, J. J. R. Targeting and Detecting Cancer Cells using Spontaneously Formed Multifunctional Dendrimer-Stabilized Gold Nanoparticles. *Analyst* **2009,** *134*, 1373-1379.
153. Dragan, A. I.; Casas-Finet, J. R.; Bishop, E. S.; Strouse, R. J.; Schenerman, M. A.; Geddes, C.

D. Characterization of PicoGreen Interaction with dsDNA and the Origin of its Fluorescence Enhancement upon Binding. *Biophys J* **2010,** *99*, 3010-3019.

154. Xu, Z.; Shen, G.; Xia, X.; Zhao, X.; Zhang, P.; Wu, H.; Guo, Q.; Qian, Z.; Wei, Y.; Liang, S. Comparisons of Three Polyethyleneimine-Derived Nanoparticles as a Gene Therapy Delivery System for Renal Cell Carcinoma. *J. Transl. Med.* **2011,** *9*, 46.
155. Doyle, S. R.; Chan, C. K. Differential Intracellular Distribution of DNA Complexed with Polyethylenimine (PEI) and PEI-Polyarginine PTD Influences Exogenous Gene Expression within Live COS-7 Cells. *Genet. Vaccines Ther.* **2007,** *5*, 11.
156. Murphy, J. E.; Uno, T.; Hamer, J. D.; Cohen, F. E.; Dwarki, V.; Zuckermann, R. N. A Combinatorial Approach to the Discovery of Efficient Cationic Peptoid Reagents for Gene Delivery. *Proc. Natl. Acad. Sci. U. S. A.* **1998,** *95*, 1517-1522.
157. Kumar, V.; Qin, J.; Jiang, Y.; Duncan, R. G.; Brigham, B.; Fishman, S.; Nair, J. K.; Akinc, A.; Barros, S. A.; Kasperkovitz, P. V. Shielding of Lipid Nanoparticles for siRNA Delivery: Impact on Physicochemical Properties, Cytokine Induction, and Efficacy. *Mol Ther Nucleic Acids* **2014,** *3*, e210.
158. Liang, B.; He, M.-L.; Xiao, Z.-P.; Li, Y.; Chan, C.-y.; Kung, H.-F.; Shuai, X.-T.; Peng, Y. Synthesis and Characterization of Folate-PEG-Grafted-Hyperbranched-PEI for Tumor-Targeted Gene Delivery. *Biochem. Biophys. Res. Commun.* **2008,** *367*, 874-880.
159. Kim, K.; Lee, H. B.; Lee, J. W.; Park, H. K.; Shin, K. S. Self-Assembly of Poly(ethylenimine)-Capped Au Nanoparticles at a Toluene-Water Interface for Efficient Surface-Enhanced Raman Scattering. *Langmuir* **2008,** *24*, 7178-7183.
160. Grabar, K. C.; Allison, K. J.; Baker, B. E.; Bright, R. M.; Brown, K. R.; Freeman, R. G.; Fox, A. P.; Keating, C. D.; Musick, M. D.; Natan, M. J. Two-Dimensional Arrays of Colloidal Gold Particles: A Flexible Approach to Macroscopic Metal Surfaces. *Langmuir* **1996,** *12*, 2353-2361.
161. Cebrián, V.; Martín-Saavedra, F.; Yagüe, C.; Arruebo, M.; Santamaría, J.; Vilaboa, N. Size-Dependent Transfection Efficiency of PEI-Coated Gold Nanoparticles. *Acta Biomater.* **2011,** *7*, 3645-3655.
162. Verma, Y. K.; Gangenahalli, G. U.; Singh, V. K.; Gupta, P.; Chandra, R.; Sharma, R. K.; Raj, H. G. Cell Death Regulation by B-Cell Lymphoma Protein. *Apoptosis* **2006,** *11*, 459-471.
163. Ding, L.; Hu, X.-M.; Wu, H.; Liu, G.-X.; Gao, Y.-J.; He, D.-M.; Zhang, Y. Combined Transfection of Bcl-2 SiRNA and MiR-15a Oligonucleotides Enhanced Methotrexate-Induced Apoptosis in Raji Cells. *Cancer Biol Med* **2013,** *10*, 16-21.
164. Gao, Y.; Wu, H.; He, D.; Hu, X.; Li, Y. Downregulation of BCL11A by SiRNA Induces Apoptosis in B Lymphoma Cell Lines. *Biomed Rep* **2013,** *1*, 47-52.

ANNEXES

ANNEX I

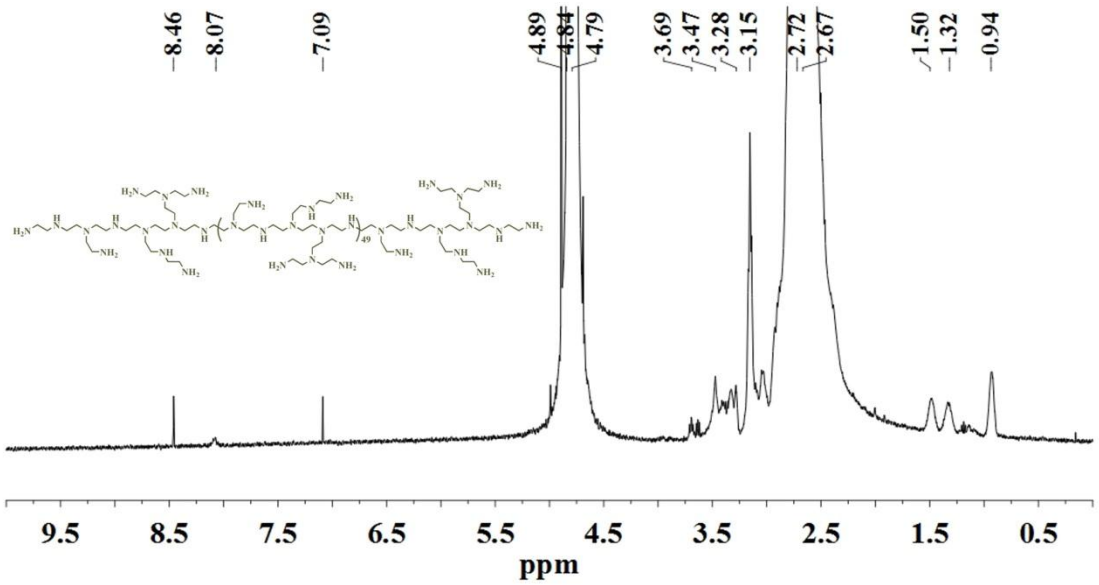

Figure 33 ^{1}H NMR spectrum of PEI in D_2O. The chemical shift at 4.79 ppm corresponds to the D_2O solvent.

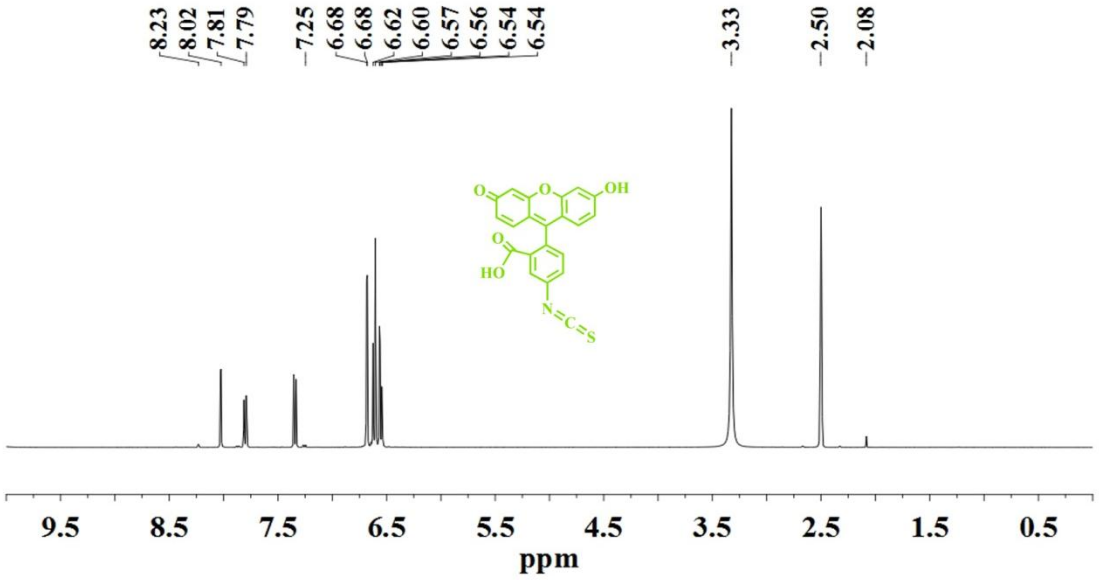

Figure 34 ^{1}H NMR spectrum of FI in DMSO. The chemical shift at 2.50 ppm corresponds to the DMSO solvent.

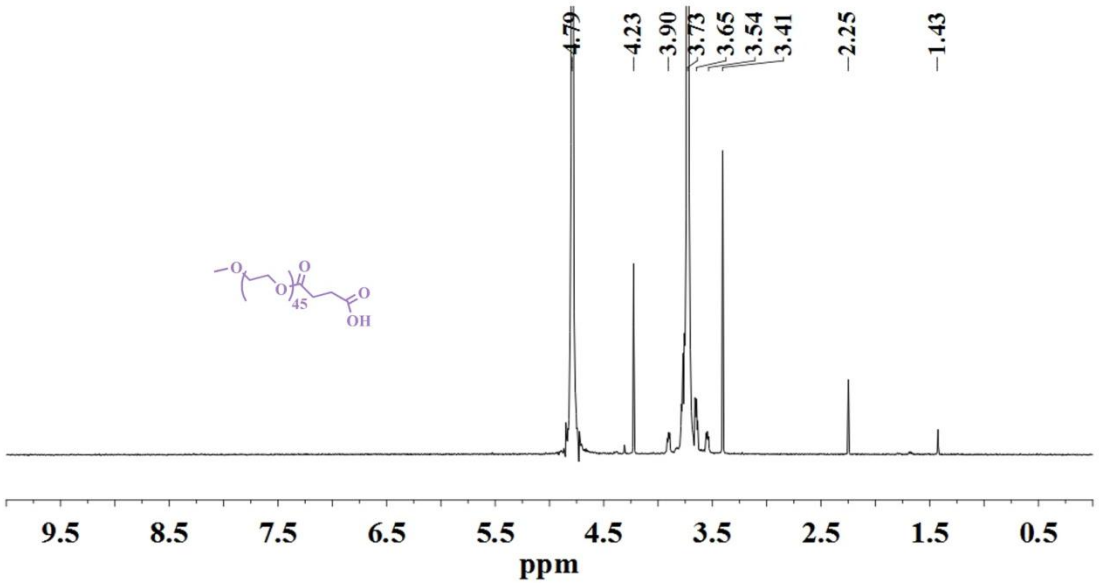

Figure 35 ^{1}H NMR spectrum of *m*PEG-COOH in D_2O. The chemical shift at 4.79 ppm corresponds to the D_2O solvent.

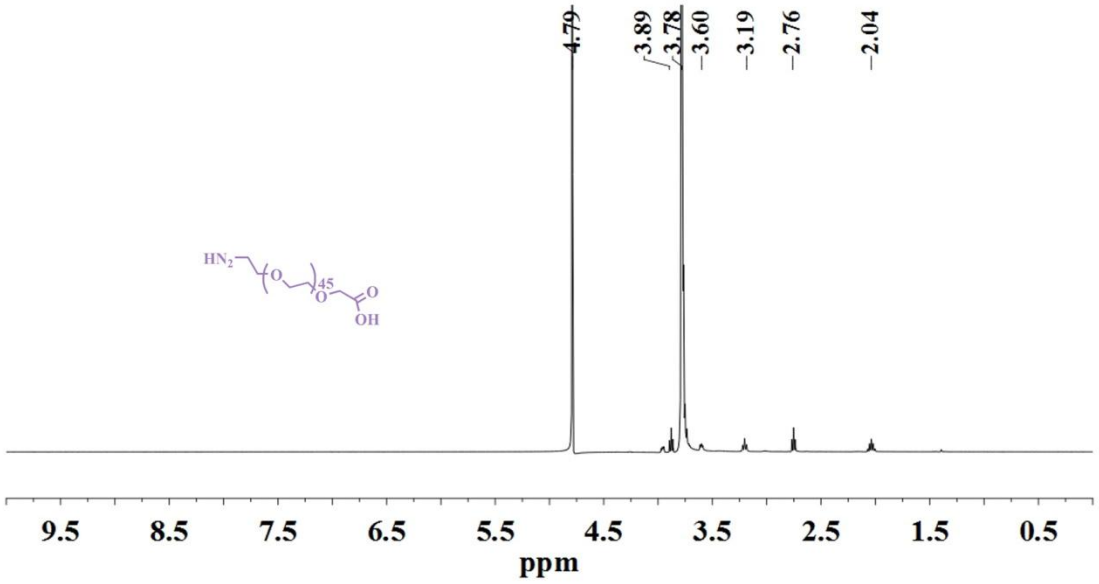

Figure 36 ^{1}H NMR spectrum of NH_2-PEG-COOH in D_2O. The chemical shift at 4.79 ppm corresponds to the D_2O solvent.

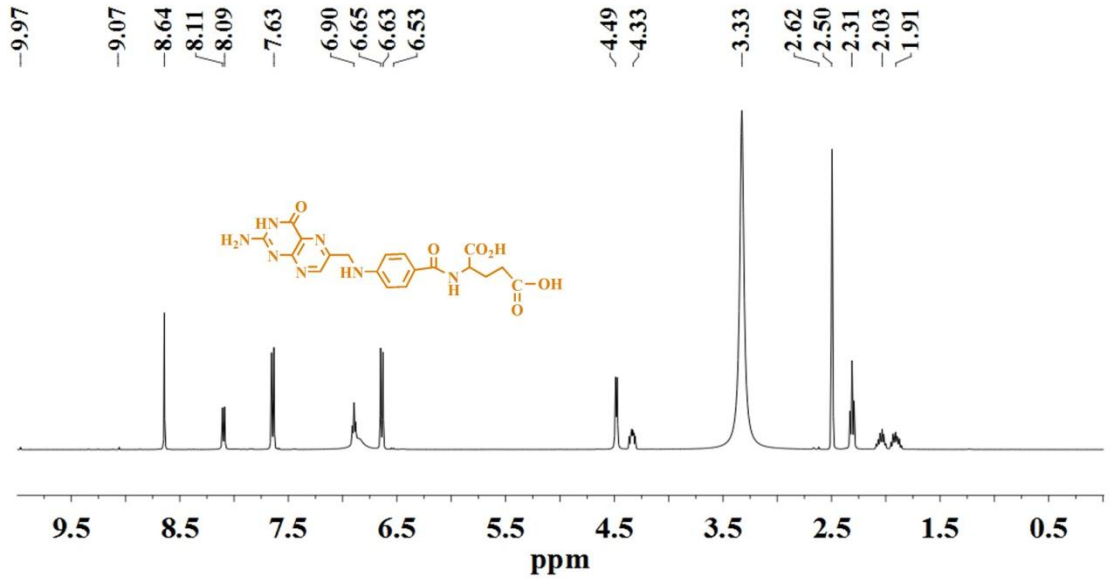

Figure 37 ^{1}H NMR spectrum of FA in DMSO. The chemical shift at 2.50 ppm corresponds to the DMSO solvent.

Table 1 Hydrodynamic size and zeta potential of the different vector/pDNA polyplexes[a].

Polyplexes of vector-pDNA	Hydrodynamic Size (nm)	Zeta Potential (mV)
PEI	290.67 ± 35.27	33.93 ± 2.44
PEI-FI-*m*PEG	319.27 ± 12.59	42.57 ± 2.66[d]
$(Au^0)_{10}$-PEI-FI-*m*PEG	223.43 ± 28.25	41.70 ± 0.88[c]
$(Au^0)_{25}$-PEI-FI-*m*PEG	203.23 ± 44.42	40.27 ± 0.42[b]
$(Au^0)_{50}$-PEI-FI-*m*PEG	360.90 ± 22.10	45.43 ± 0.45[d]
PEI-FI-(PEG-FA)	164.07 ± 3.47	40.77 ± 1.48[c]
$(Au^0)_{10}$-PEI-FI-(PEG-FA)	138.23 ± 12.24	42.23 ± 0.90[c]
$(Au^0)_{25}$-PEI-FI-(PEG-FA)	171.10 ± 31.40	40.00 ± 1.93[b]
$(Au^0)_{50}$-PEI-FI-(PEG-FA)	157.03 ± 4.30	41.33 ± 1.08[c]

[a] Results are mean ± SD of three independent sample measurements.

[b] $p<0.05$, when compared with PEI-pDNA polyplexes.

[c] $p<0.01$, when compared with PEI-pDNA polyplexes.

[d] $p<0.001$, when compared with PEI-pDNA polyplexes.

Table 2 Hydrodynamic size and zeta potential of the different vector/siRNA complexes[a].

Complexes of vector/siRNA	Hydrodynamic Size (nm)	Zeta Potential (mV)
PEI	338.43 ± 31.75	25.43 ± 1.20
PEI-FI-*m*PEG	426.90 ± 52.94	25.90 ± 2.47
$(Au^0)_{50}$-PEI-FI-*m*PEG	426.00 ± 22.55	23.83 ± 0.17
PEI-FI-(PEG-FA)	420.27 ± 79.60	24.23 ± 1.47
$(Au^0)_{50}$-PEI-FI-(PEG-FA)	260.10 ± 65.75	22.80 ± 1.50

[a] Results are mean ± SD of three independent sample measurements.

[b] $p<0.05$, when compared with PEI-siRNA complexes.

[c] $p<0.01$, when compared with PEI-siRNA complexes.

[d] $p<0.001$, when compared with PEI-siRNA complexes.

União Europeia

Governo da República Portuguesa

Região Autónoma da Madeira